Meteosat Surface Albedo Retrieval: Algorithm Theoretical Basis Document

Doc.No. : EUM/OPS/SPE/12/3367
Issue : v3B e-signed
Date : 23 March 2016
WBS/DBS :

EUMETSAT
Eumetsat-Allee 1, D-64295 Darmstadt, Germany
Tel: +49 6151 807-7
Fax: +49 6151 807 555
http://www.eumetsat.int

Document Change Record

Issue / Revision	Date	DCN. No	Changed Pages / Paragraphs
1.0	August 1998		Initial Issue (PDF only). Document issued jointly by DG JRC-SAI and EUMETSAT Also registered as: JRC Publication No. EUR 18130 EN
2.0	22 November 2013		Initial issue under EUMETSAT Document Control Added Symbol explanation tables and new reference sections. Added section defining and describing the Atmospheric Scattering Module (ASM) Added Reference Document listing and annotations. Added numbering scheme to all equations.
v2A	4 April 2014		Document read-only for scientific review before release.
v2B	29 April 2014		Comments from technical team review incorporated.
v3	15 December 2015		New version created before further technical team review.
v3A	16 February 2016		Added new details in Section 4.4 on generation of BRF from MSA product.
v3B	23 March 2016		New version created following revision of reference table.

Table of Contents

Table of Figures

Table of Tables

1 INTRODUCTION

1.1 Purpose

This Algorithm Theoretical Basis Document (ATBD) describes the algorithm used to retrieve surface albedo over terrestrial surfaces from the visible channel of the MVIRI instrument onboard Meteosat First Generation (MFG) satellites. The algorithm is applied to all MFG mission data archived at EUMETSAT.

1.2 Scope

This ATBD defines the physical principles and mathematical background supporting the proposed approach. It gives a detailed description of the algorithm to be implemented and presents the assumptions and limitations of the approach. This document also identifies the sources of input data, including the auxiliary data, and the products generated during processing.

1.3 Document Structure

Section	*Contents*
Section 1	Contains the document purpose and scope, as well as references to all foundation documents and references.
Section 2	Contains an overview of the science, definitions used in the document, a description of the instrument used and the strategy employed.
Section 3	Describes the algorithm and goes into detail about each module that is involved in the process.
Section 4	A broad listing of the assumptions and limitations involved in this theoretical basis document.
Appendix A	Product List
Appendix B	A description of the Computed RAdiative transfer Functions (CRAF) database.
Appendix C	Explains all the integrals mentioned in the ATBD and includes a numerical solution using a Gaussian quadrature method.
Appendix D	Contains a table of the scalable parameters.
Appendix E	Tables in this section illustrate each mathematical symbol and shorthand representation used in the document.

1.4 Reference Documents

Number	*Author, title, reference*
RD 1	Avissar, R. and M. M. Verstraete (1990). *The representation of continental surface processes in mesoscale atmospheric models.* Reviews of Geophysics, **28**, 35-52.
RD 2	Cabot, F. and G. Dedieu (1997). *Surface albedo from space: Coupling bidirectional models and remotely sensed measurements.* Journal of Geophysical Research, **16**, 19645-19664.
RD 3	Dickinson, R. E. (1983). *Land surface processes and climate-surface albedo and energy balance.* Advances in Geophysics, **25**, 305-353.
RD 4	Diner, D. J., W. A. Abdou, A. T. P., K. Crean, H. R. Gordon, R. A. Kahn. J. V. Martonchik, S. R. Paradise, B. Pinty, M. M. Verstraete, M. Wang, and R. A. West (1997). *MISR Level 2 Aerosol Retrieval Algorithm Theoretical Basis. Technical Report* JPL D-11400, Rev. C, NASA, Jet Propulsion Laboratory.
RD 5	Engelsen, O. B. Pinty, M. Verstraete, and J.V. Martonchik (1996). *Parametric bidirectional reflectance factor models: Evaluation, improvements and applications*. Technical Report EU 16426 , EC Joint Research Centre.
RD 6	GCOS (2011): Systematic Observation Requirements for Satellite-based Data Products for Climate, 2011 Update, Supplemental details to the satellite-based component of the "Implementation Plan for the Global Observing System for Climate in Support of the UNFCCC (2010 Update)", GCOS – 154.
RD 7	Govaerts, Y.M. (1999). *Correction of the Meteosat-5 and-6 VIS band relative spectral response withMeteosat-7 characteristics.* Int Journal of Remote Sensing, **20**, 3677–3682.
RD 8	Govaerts, Y.M.; Clerici, M.; Clerbaux, N. (2004): *Operational calibration of the Meteosat radiometer VIS band.* IEEE Transactions on Geoscience and Remote Sensing, **42**, No.9, pp. 1900- 1914, doi: 10.1109/TGRS.2004.831882
RD 9	Govaerts, Y.; Pinty, B.; Taberner, M.; Lattanzio, A. Spectral conversion of surface albedo derived from Meteosat first generation observations. IEEE Geosc. Rem. Sens. Letters 2006, 3, 23–27.
RD 10	Govaerts, Y., and Lattanzio, A. (2007). *Retrieval Error Estimation of Surface Albedo Derived from Geostationary Large Band Satellite Observations: Application to Meteosat-2 and -7 Data.* Journal of Geophysical Research, **112**, doi:10.1029/2006JD007313
RD 11	Henderson-Sellers, A. and M. F. Wilson (1983*). Surface albedo data for climatic modeling*. Reviews of Geophysics and Space Physics, **21**, 1743-1778.
RD 12	Holben, B. T. Eck, I. Slutsker, D.Tanre, J. Buis, A. Setzer, E.Vermote, J. Reagan, Y. Kaufman, T. Nakajima, F. Lavenu, I. Jankowiak, and A. Smirnov (1998): *AERONET-a federated instrument network and data archive for aerosol characterization*. Remote Sensing of Environment, **66**, 1–16.
RD 13	Kaufman, Y. J. and C. Sendra (1988). *Algorithm for atmospheric corrections.* International Journal of Remote Sensing, **9**, 1357-1381.
RD 14	King, M. D., Y. J. Kaufman, M. W. P., and D. Tanrè (1992): *Remote sensing of cloud, aerosol, and water vapor properties from the moderate resolution imaging spectrometer (MODIS).* IEEE Transactions Geoscience and Remote Sensing, **30**, 2-27.
RD 15	Lattanzio, A., Y. Govaerts, et al. (2006). *Consistency of surface anisotropy characterization with Meteosat observations.* Advanced Space Research, doi:10.1016/j.asr.2006.02.049.
RD 16	Lenoble, J. (1985). *Radiative transfer in scattering and absorbing atmospheres: standard computational procedures*. Hampton, VA, USA: A. Deepak Publishing.

Number	*Author, title, reference*
RD 17	Loew, A. And Y.Govaerts (2010). *Towards multi-decadal consistent Meteosat surface albedo time series.* Remote Sensing, **2(4)**, 957–967.
RD 18	Martonchik, J. V., D. J. Diner, R. A. Kahn, T. P. Ackerman, M. M. Verstraete, B. Pinty, and H. R. Gordon (1998). *Techniques for the retrieval of aerosol properties over land and ocean using multi-angle imaging.* IEEE, Trans Geoscience and Remote Sensing, **36**, 1212-1227.
RD 19	EUMETSAT (2011): Meteosat First Generation User Handbook. Available from ops@eumetsat.int, 40pp.
RD 20	Nicodemus, F. E., J. C. Richmond, J. J. Hsia, 1. W. Ginsberg, and T. Limperis (1977): *Geometrical considerations and nomenclature for reflectance. NBS Monograph 160*, National Bureau of Standards, U.S. Department of Commerce, Washington, DC.
RD 21	Ohring G., Wielicki B., Spencer R., Emery B., and Datla R. (2005): *Satellite Instrument Calibration for Measuring Global Climate Change – Report of a Workshop.* Bulletin of the American Meteorological Society, September 2005, 1303-1313.
RD 22	Pinty, B. and D. Ramond (1987). *A method for the estimate of broadband directional surface albedo from a geostationary satellite.* Jour Climate and Applied Meteorology, **26**, 1709-1722.
RD 23	Pinty, B., Roveda, F., Verstraete, M.M., Gobron, N., Govaerts, Y., Martonchik, J.V., Diner, D.J., and Kahn, R.A. (2000a) *Surface albedo retrieval from Meteosat: Part 1: Theory,* Journal of Geophysical Research, **105**, 18099-18112.
RD 24	Pinty, B., Roveda, F., Verstraete, M.M., Gobron, N., Govaerts, Y., Martonchik, J.V., Diner, D.J., and Kahn, R.A. (2000b) Surface albedo retrieval from Meteosat: Part 2: Applications, Journal of Geophysical Research, **105**, 18113-18134.
RD 25	Pinty, B., Lattanzio, A., Martonchik, J. V., Verstraete, M. M., Gobron, N., Taberner, M., Widlowski, J.-L., Dickinson, R. E., and Govaerts, Y. (2005). *Coupling diffuse sky radiation and surface albedo.* J Atm. Science, **62**, 2580-2591.
RD 26	Press, "V. H., B. P. Flannery, S. A. Teulkosky, and W. T. Vetterling (1988). *Numerical Recipes in C, 1st edition.* Cambridge, USA: Cambridge University
RD 27	Privette, J. 1., T. F. Eck, and D. W. Deering (1997). *Estimating spectral albedo and nadir reflectance through inversion of simple BRDF models with AVHRR/MODIS-like data.* Journal of Geophysical Research, **102**, 29, 529-542.
RD 28	Rahman, H., B. Pinty, and M. Verstraete (1993). *Coupled surface-atmosphere reflectance (CSAR) model. 2. Semiempirical surface model usable with NOAA Advanced Very High Resolution Radiometer data.* Journal of Geophysical Research, **98**, 20, 791-20,80l.
RD 29	Schaaf, C. B., and Coauthors, (2002): *First operational BRDF, albedo and nadir reflectance products from MODIS.* Remote Sens. Environ., **83**, 135–148.
RD 30	Schmetz, J., P. Pili, S. Tjemkes, D. Just, J. Kerkmann, S. Rota, and A. Ratier, 2002: An introduction to Meteosat Second Generation (MSG). Bull. Amer. Meteor. Soc., 83, 977–992.
RD 31	U.S. Standard Atmosphere, 1962 (1962), U.S. Government Printing Office, Washington, DC
RD 32	Vermote, E., D. Tamrè, J. L. Deuze, M. Herman, and M. J. J. (1997). *Second simulation of the satellite signal in the solar spectrum: An overview. I*EEE Trans. Geoscience Remote Sensing, **35**-3, 675-686.

1.5 Abbreviations and Acronyms used in this document

Acronym	*Meaning*
AGFI	Absorbing Gas Fields
AI	Atmosphere Identifier
ASSF	Average Surface Shape Factor
ASI	surface Anisotropy Shape Indicator
ASM	Atmospheric Scattering Module
ATBD	Algorithm Theoretical Basis Document
BHR	Bi-Hemispherical Reflectance
BHR-iso	Bi-Hemispherical Reflectance isotropic conditions
BRF	Bidirectional Reflectance Factor
BRDF	Bidirectional Reflectance Distribution Function
BSI	TOA BRFs Structure Indicator
BSRF	Black Surface Reflectance Factor
CLMA	CLoud Mask
CM	Cloud Mask
CRAF	pre-Computed Radiation transfer Functions
DATF	Direct Attenuation Transmission Factor
DBHR	Daily Averaged Bi-hemispherical Reflectance
DCP	Data Consistency Procedure
DCPf	Data Consistency Procedure flag
DDHR	Daily Averaged Hemispherical Reflectance
DHR	Directional Hemispherical Reflectance
DIM	Data Interpretation Model
DQI	Data Quality Indicator
DSM	Data Selection Module
IDFT	Incoming Diffuse Transmission Factor
LUT	Look Up Table
MFG	Meteosat First Generation
MPEF	Meteorological Products Extraction Facility
MRPV	Modified Rahman-Pinty-Verstraete model
MSA	Meteosat Surface Albedo
MVIRI	Meteosat Visible and Infra Red Imager
NESC	Number of remaining slots after the DCP
NREM	Number of slots removed by the DCP
NSLOT	Minimum number of slots required for the inversion
OGTF	Other Gases Transmission Factor

Acronym	*Meaning*
OLAM	Ocean-Land Mask Dataset
OTF	Ozone Transmission Factor dataset
RCF	Retrieved Configuration File
RPV	Rahman-Pinty-Verstraete model
SVAT	Soil-Vegetation-Atmosphere-Transfer
STF	Scattering Transmission Factor dataset
TOA	Top Of Atmosphere
TOFI	Topographic Fields dataset
TOMS	Total Ozone Mapping System
TOPO	TOPOgraphic flag
WVTF	Water Vapour Transmission Factor dataset
6S	Second Simulation of the Satellite Signal in the Solar Spectrum

2 SCIENTIFIC OVERVIEW

The bulk of the solar radiation available to the Earth system is absorbed at or near the oceanic and continental surface, and then ultimately released to the atmosphere through the fluxes of infrared radiation, as well as sensible and latent heat. The fraction of solar energy absorbed at the surface of the planet is controlled by its surface albedo, which is highly variable in space and time over terrestrial surfaces. To ensure adequate representation of land-surface processes and their interactions with the atmosphere, it is therefore necessary to estimate accurately land surface albedo values at the appropriate time and space scales (see for instance, Dickinson 1983 [RD 3], and Avissar and Verstraete 1990 [RD 1]. In the early 1980s, it was suggested that an absolute accuracy of 0.05 for spatial and temporal scales compatible with climate studies was desirable (see Henderson-Sellers and Wilson 1983 [RD 11]). Despite the recognized importance of the objective, the scientific community has not yet succeeded in this endeavour to the extent that, for instance, surface albedo maps are not routinely provided by meteorological centres–or by any other national or international entity for that matter. Paradoxically, the off-line modelling of land-surface processes, for instance in Soil-Vegetation-Atmosphere-Transfer schemes (SVATs), has been significantly improved, and these surface representations are beginning to be integrated in meteorological and climate forecast models. A strong demand for reliable and accurate information on many land surface properties and surface albedo in particular thus remains.

Satellite-borne instruments constitute *a priori* a unique tool for monitoring surface albedo values at the global scale and at spatial and temporal resolutions adequate for meteorological and climate studies. However, the above assertion implies that the problems hindering the accurate estimation of surface albedo values are correctly addressed. The radiative contributions to the measured radiances due to the atmospheric layers and the variations due to the anisotropic reflectance of all terrestrial surfaces are of primary concern in this context (Pinty and Ramond 1987 [RD 22]). In principle, the surface albedo could be estimated rather accurately if the radiative properties of the atmosphere were known at the same time and location as an extensive multi-angular and multispectral sampling of the radiance fields emerging from the Top of the Atmosphere (TOA) were gathered in space. Although some of the atmospheric radiative properties (for instance the total ozone and water vapour contents) are known with sufficient accuracy, others, such as the aerosol load and properties, are not yet measured routinely.

Fundamentally, the spectral radiance derived from a satellite measurement is controlled by all the radiative processes with which the solar radiation has interacted through the various parts of the atmosphere and the underlying surface during its travel. In fact, satellite measurements correspond to one of the four boundary conditions of the atmospheric radiative problem: the first one is the radiation from the sun which acts as the source of energy and is assumed to be known, the second is the downward radiance field reaching the surface, and the third one is the upward radiance field at the bottom of the atmosphere. Estimating the land surface albedo from satellite measurements thus implies the estimation of the two unknown boundary conditions at the surface. The crux of the problem is to interpret the measured upward radiance field at the surface so that the contribution from the surface scattering properties is accurately de-convolved from that of the atmosphere. Since the atmospheric aerosol properties strongly impact radiation transfer processes at solar wavelengths and they are not independently available as an operational product, one possible approach can aim at retrieving both surface and atmospheric (aerosol) properties simultaneously from the remote sensing data by inverting coupled surface-atmosphere radiation transfer models against these data. As is usually the case when solving an inverse problem, it is necessary to ensure that sufficient input data

are available and that a minimum set of critical variables are estimated to guarantee an accurate and reliable assessment of the retrieved properties.

Surface albedo can be defined spectrally or for spectral bands of finite width with broadband albedo generally referring to the entire 0.3 – 3.0 µm range or the two broadband ranges 0.3 – 0.7 µm and 0.7–3.0 µm. The algorithm presented in this Algorithm Theoretical Base Document (ATBD) focuses on the retrieval using measurements taken with the Meteosat Visible and Infra Red Imager (MVIRI) Visible band (see Figure 1), on board Meteosat First Generation (MFG) satellites. Such a spectral surface albedo can be converted into a broadband value following Loew and Govaerts (2010) [RD 17].

Two simple definitions for the surface albedo, corresponding to extreme conditions, have been defined in Schaaf et al. 2002 [RD 29]:

- *Black sky albedo*, technically known as the directional hemispherical reflectance factor (DHR), is the reflectance of a surface when the illumination comes from a single direction. Black sky albedo is the albedo in the absence of any atmosphere. It depends on the angular position of the source of light and on surface properties;
- *White sky albedo*, technically known as bi-hemispherical reflectance factor under isotropic illumination (BHR_{iso}), is the reflectance of a surface when the irradiance is isotropic. The surface albedo under an overcast homogeneous cloud deck would be a good approximation of white sky albedo. This value depends only on surface properties.

In practice, the actual instantaneous albedo of a land surface is often approximated from a linear combination of the black and white sky albedo, where the weighting factors are the relative proportions of direct and isotropic diffuse radiation. Such a combination is sometimes referred to as the *blue sky albedo*. It depends on the angular position of the main source of illumination for direct radiation, the atmospheric condition, and on surface properties. The retrieval scheme described in this ATBD is only generating Black and White Sky albedo (the only parameters one can retrieve from satellite observations). The blue sky albedo can be obtained as explained in Pinty et al. 2005 [RD 25].

Variable/ Parameter	*Horizontal Resolution*	*Vertical Resolution*	*Temporal Resolution*	*Accuracy*[1]	*Stability*[2]
Black-sky albedo	1 km	N/A	Daily to weekly	max (5%; 0.0025)	max (1%; 0.0001)
White-sky albedo	1 km	N/A	Daily to weekly	max (5%; 0.0025)	max (1%; 0.0001)

Table 1: GCOS target requirements from GCOS (2011)

Table 1 provides requirements from GCOS (2011) that represent the target for the construction of a Climate Data Record from observations coming from many instruments over time. Complete requirements can be found on the GCOS website http://www.wmo.int/pages/prog/gcos/index.php.

The GCOS rationale behind the numbers in Table 1 is to detect the change in radiative forcing that is equivalent to 20 per cent of the expected total change in radiative forcing per decade due to greenhouse gases and other forcing, for example, ~0.1 Wm^{-2} per decade which is a definition originating from Ohring (2005) [RD 21]. These requirements need to be understood in order to build a global surface albedo product that combines different observing systems into a Climate Data Record.

[1] Accuracy: degree of closeness of measurements of a quantity to that quantity's actual (true) value.

[2] Stability: estimation of measurement consistency over time.

Surface albedo retrieval schemes applied to individual observing systems such as Meteosat First Generation are not expected to fulfil these requirements but deliver useful data for many climate applications, for example those applications associated with climate modelling where the data can be used as boundary condition.

The design of the MVIRI does not yield an adequate spectral and directional sampling of the radiance fields scattered by the Earth. However, thanks to its geostationary orbit, this sensor is able to sample the TOA emerging radiance field every thirty minutes during the course of the day, i.e., for different solar illumination conditions. In other words, if the geophysical system under investigation does not change drastically during the daily period of solar illumination, Meteosat data provide a useful angular sampling of the radiance fields scattered by the Earth system. Whenever and wherever this assumption is valid, the Meteosat temporal sampling of the radiance field for a given location can thus be interpreted as an angular sampling: this approach constitutes the corner stone of the strategy for the estimation of surface albedo values. The objectives of the Meteosat Surface Albedo (MSA) retrievals are as follows:

- to estimate daily surface albedo values over most of the terrestrial surfaces sampled by Meteosat;
- to characterize the surface brightness and anisotropy using a set of three *ad hoc* parameters (defined in Section 3.6.2);
- to provide a simultaneous daily estimation of probable aerosol load radiatively compatible with the corresponding surface products;
- to provide an estimation of the uncertainly for the surface albedo and aerosol load along with the retrieval.

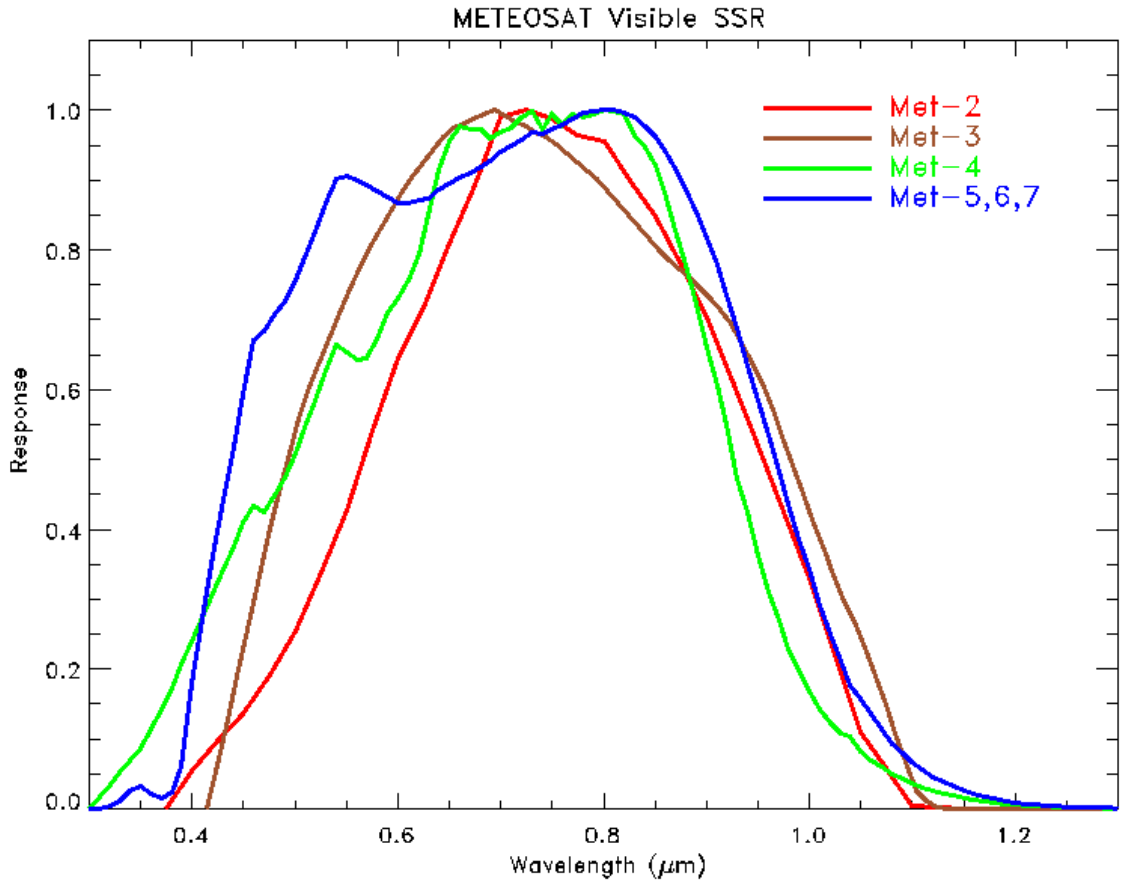

Figure 1: Meteosat First Generation MVIRI Visible channel Sensor Spectral Response (SSR)

2.1 Instrument characteristics

The technical characteristics of the Meteosat series of instruments and their orbital positions can be found in the Meteosat First Generation User Handbook [RD 19]. For the purpose of this document, it will be enough to recall that Meteosat is sampling the radiation field emitted by Earth every thirty minutes in three spectral channels distributed over the visible solar range, the thermal infrared and the water vapour channels, respectively. The present project only uses geographically rectified data (level 1.5) acquired by one Meteosat visible channel, calibrated with the information provided by EUMETSAT. The Meteosat visible channel scans the Earth disk into a matrix of 5000 × 5000 pixels, corresponding to a spatial resolution of 2.5 km at the sub-satellite point, in about 30 minutes. The pixel becomes larger in relation to its distance from the SSP, this enlargement means that the pixel will cover surfaces with different reflectance characteristic. This is not considered in the retrieval strategy. The visible channel is sensitive to radiation scattered from about 400–1100 nm and exhibits a maximum response between 700 nm –800 nm. These latter values as well as the shape of the sensor response are slightly different between the various Meteosat instruments. See Figure 1 and Govaerts at al., 2004 [RD 8]. The data acquired by this series of instruments are therefore sensitive to the amount of absorbing gases exhibiting absorption bands in this spectral region, in particular to ozone and water vapour.

2.2 Retrieval Strategy

The Meteosat Surface Albedo (MSA) algorithm relies on an approach proposed by Pinty et al. 2000a, 2000b [RD 23] and [RD 24]. The algorithm accumulates during the course of the day geostationary cloud free observations acquired in the visible part of the electromagnetic spectrum at different illumination conditions to retrieve the surface anisotropy and the atmospheric aerosol load through the inversion of a Radiative Transfer Model (RTM) as shown in Figure 2. This retrieval scheme relies on the applicability of the reciprocity principle at a spatial scale of several km (Lattanzio et al., 2006 [RD 10]). Assuming that the geophysical properties controlling the radiance field emerging from a given pixel do not evolve much over a day, the acquisition of radiance data over such a period of time corresponds to an angular sampling of the same radiance field for various solar geometries. Such a strategy had already been explored by Pinty and Ramond (1987) [RD 22] to study the seasonal variation of surface albedo over the Sahelian regions. However, this assumption is not sufficient to guarantee that an accurate retrieval of surface parameters can be achieved on the basis of Meteosat data alone, because the number of unknown geophysical variables of the problem, both within the atmosphere and at the surface, remains too high. It is therefore necessary to further constrain the surface retrievals by taking advantage of other currently available knowledge on the coupled surface-atmosphere system. The proposed algorithm will use ozone and water vapour contents from other sources as input data to reduce the radiation transfer problem to a surface-aerosol scattering problem. The most critical variables of such a system are then the aerosol optical depth and the surface brightness. Indeed, it will be assumed that actual atmospheric situations will match one of the limited numbers of standard atmospheric models which can be prescribed *a priori*, and that the only free atmospheric property to be estimated in the retrieval process is the aerosol load. The surface brightness will similarly be estimated during the same retrieval process from a set of predefined solutions which describe the anisotropic properties of typical surfaces. The approach that is followed in solving this surface-aerosol scattering problem is an extension of the MISR algorithm for retrieving aerosol optical depth values over dark surfaces (Diner et al. 1997 [RD 18]).

A 10-day composite of the daily surface albedo maps is performed to minimise the impact of cloud coverage, particularly in the tropical regions. The algorithm also estimates retrieval errors and provides a probability for the retrieval (Govaerts and Lattanzio, 2007 [RD 10]) defined according to the quality of the fit and the actual number of available observations.

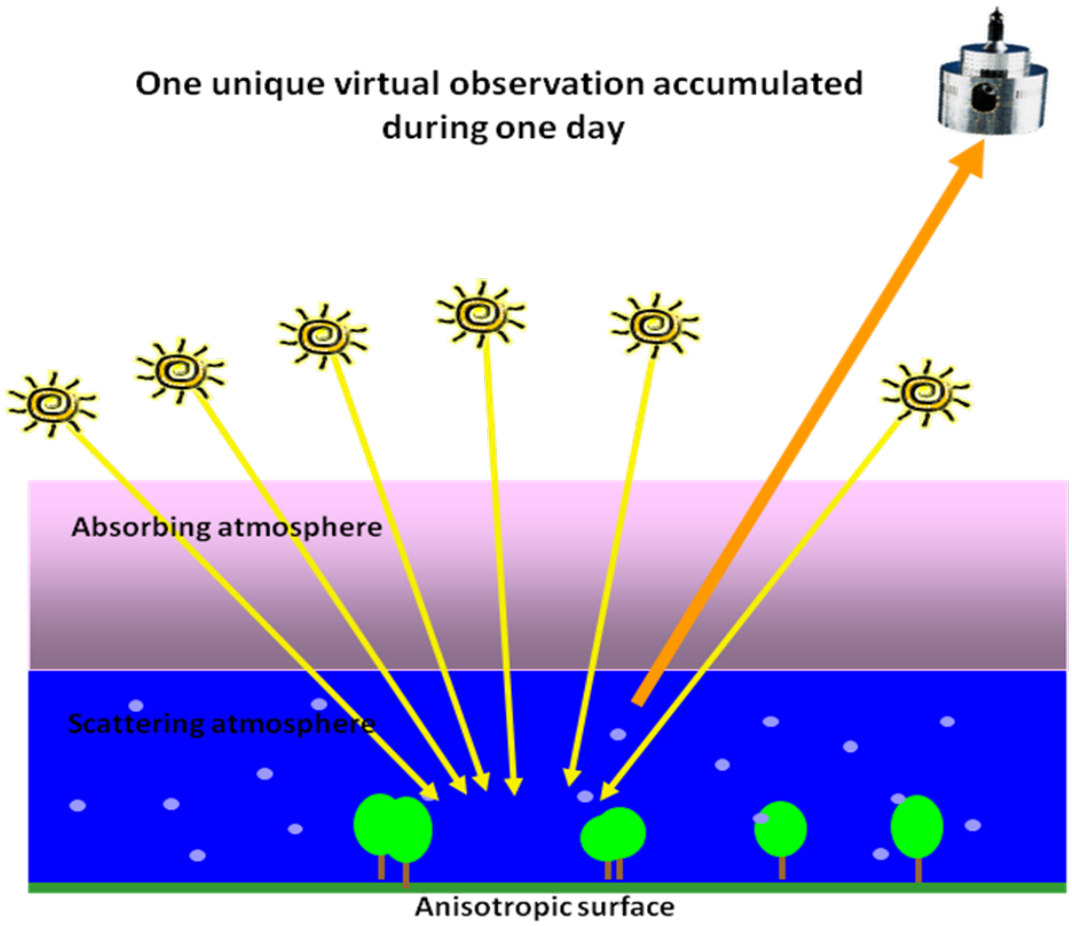

Figure 2: MSA Retrieval scheme. The observations accumulated during the day are used as an angular sampling of the surface.

2.3 Delivered products

For each 10-day compositing periods, the following quantities are produced:

- the Directional Hemispherical Reflectance (DHR) considering a Sun zenith angle of 30°;
- the isotrōpic Bi-Hemispherical Reflectance $BHR_{iso;}$
- average Aerosol Optical Thickness (AOT), and
- retrieval uncertainty.

3 ALGORITHM DESCRIPTION

3.1 Processing Outline

The complete surface albedo algorithm process includes two main processing steps: the daily accumulation of the required input data (the box in the upper left of Figure 3) and the retrieval of the data (the larger DPM panel in Figure 3. The figures that follow will break this figure into its components.

The first step in the process takes place in the Data Accumulation Module (DAM). The daily Top of Atmosphere measurements for each pixel are stored in files called DAM files together with any other dynamical or static ancillary information needed for the retrieval. Dynamic and static input files are described in 0 and 3.2.1.

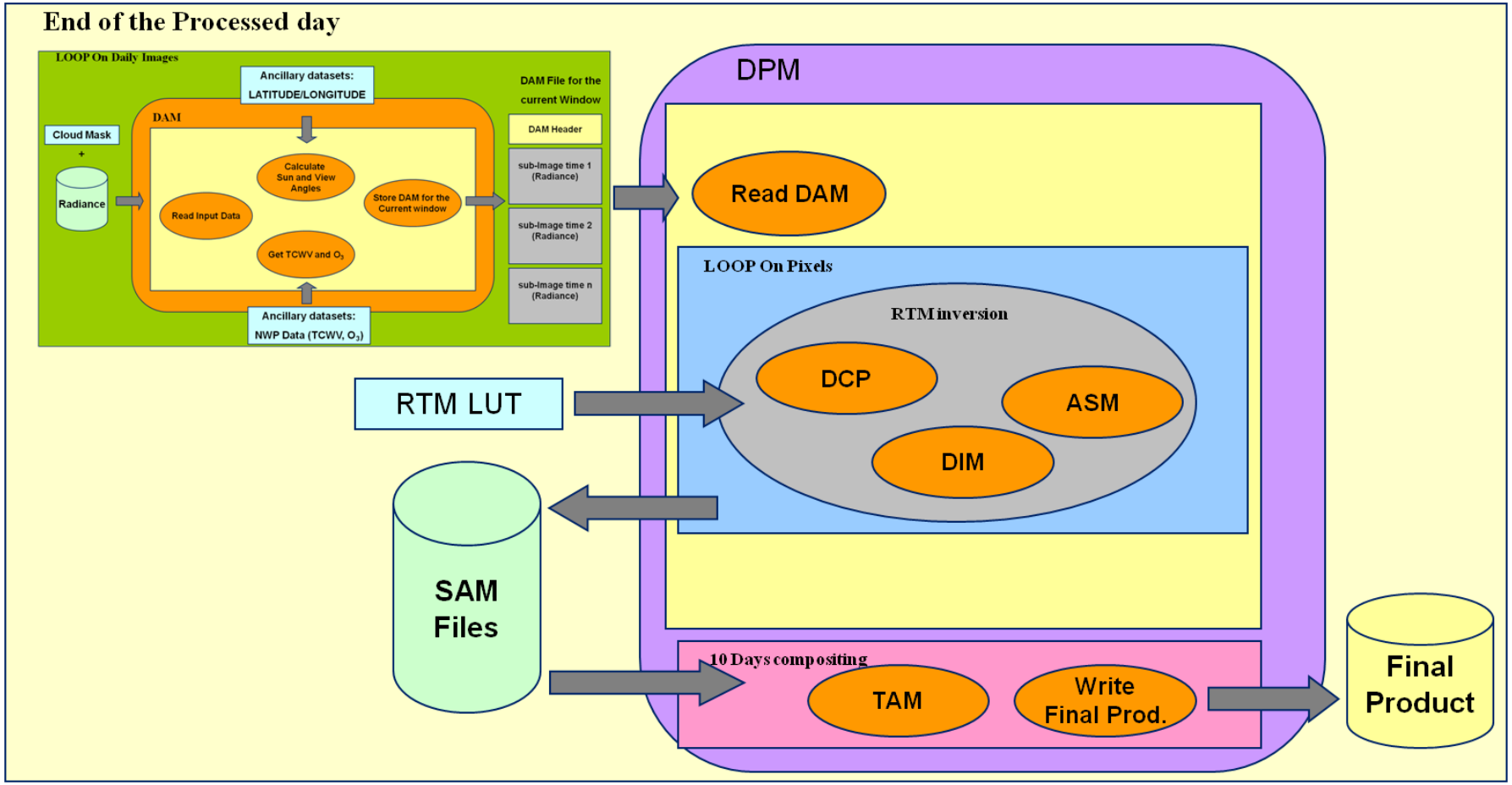

Figure 3: MSA Complete algorithm processing steps.

The first step in the process takes place in the Data Accumulation Module (DAM). The daily Top of Atmosphere measurements for each pixel are stored in files called DAM files together with any other dynamical or static ancillary information needed for the retrieval. Dynamic and static input files are described in 0 and 3.2.1.

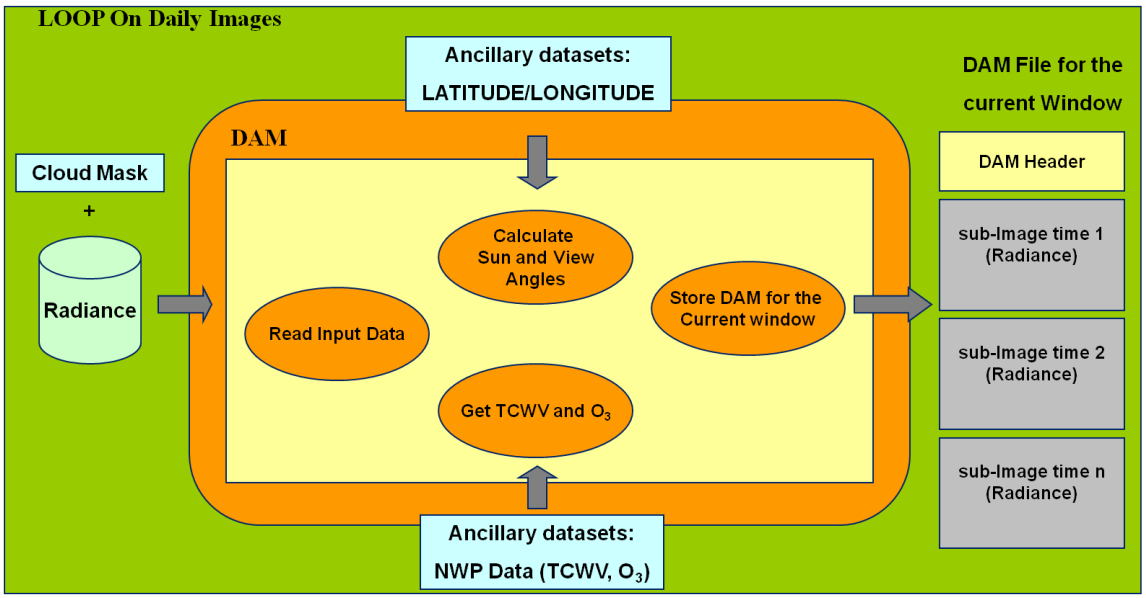

Figure 4: Daily Accumulation Model (DAM): functionalities and interface

In step two of the process, the retrieval is done in the Data Processing Module (DPM). To speed up the retrieval, the field of solutions for the RTM is discretised and all the necessary integrals for of the radiative transfer equations are stored in Look-up Tables. Once a solution (if any) for each pixel is determined, the retrieval information is stored in the Space Averaging Module (SAM) files. Finally, among all the solutions retrieved for the 10-day period, one is selected and stored in the final product.

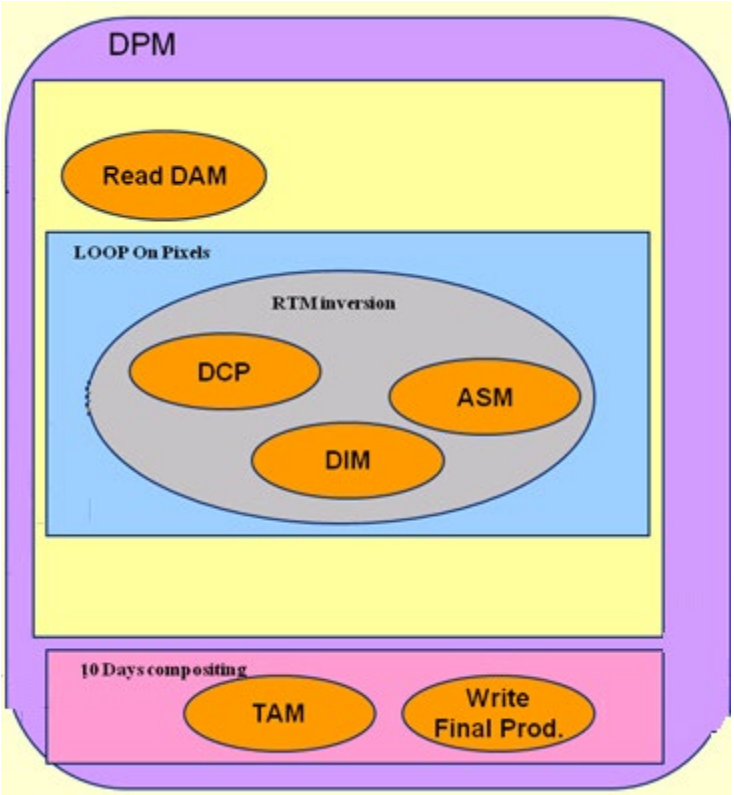

Figure 5: Data Processing Model layout

This retrieval approach described in details in Pinty et al., 2000a and 2000b [RD 23] is implemented in the following four steps in the DPM:

- **Data Consistency Procedure (DCP):** This module is responsible for screening out the cloudy pixels and it must be executed before entering the Atmospheric Scattering Module. This procedure runs for every pixel. If a cloud mask is available (Optional input), it is applied prior to the DCP process;
- **Atmospheric Scattering Module (ASM):** In this module, the gas absorption contribution to the TOA reflectance is removed and the inversion of the RTM representing the scattering layer and surface reflectance for all the possible values of the parameterised fields (see Govaerts and Lattanzio, 2007 [RD 10]) is performed;
- **Data Interpretation Module (DIM):** In this module, the most likely solution among all the possible ones estimated in the previous step for each pixel is chosen;
- **Space-Time Averaging Module (TAM):** Steps 1 to 3 are applied after the daily accumulation and the solutions stored in the SAM temporary files for the subsequent 10-day temporal compositing. In this latter module, the best solution for the 10-day period is selected.

3.2 Algorithm information input

The MSA input can be divided in dynamic and static ancillary input files. The dynamic input files are listed in Dynamic Input Files

File	*Meaning*	*Units*
Radiance	Radiance at pixel resolution retrieved in the instrument visible band	Wm^{-2} sr^{-1}
Cloud Mask	Cloud mask at pixel level. If not present, the algorithm assumes all pixels are cloud-free. 0: Cloud free, 1: Cloudy	1
NWP Model Reanalysis Data	Total Column Ozone (TCO3) Total Column Water Vapour (TCWV). If not present, default values are used : TCO3: 0.3cm atm, TCWV: 2.0 gcm^{-2}	TCO3: (cm atm) See ***Note*** below. TCWV: gcm^{-2}

Note: 1 DU (Dobson Unit) = 0.001 cm atm: 0.3cm atm = 300 DU

Table 2: GSA dynamic input files

The NWP data, the Total Column Ozone (TCO3) and Total Column Water Vapour (TCWV) are used in one of the Look-Up Tables (LUT) in order to invert the Radiative Transfer Model (RTM). Several ozone and water vapour bands are located within the Meteosat visible spectral response and the effects of these gases on radiation transfer processes must be considered. The sensitivity of the proposed retrieval schemes with respect to those atmospheric parameters has been analysed by Pinty et al. (2000b) [RD 24].

3.2.1 Static Input Files

The Ancillary static input files are listed in Table 3. The Latitude and Longitude input files are generated according to the MVIRI-rectified image definition. The content of the LUTs is specified in Section 3.9.

File	*Meaning*
Look Up Table (LUT)	Binary files. The LUTs contain pre-computed functions and parameters needed for the inversion of the radiative transfer model (see section Appendix A)
Latitude	MVIRI rectified image coordinates
Longitude	MVIRI rectified image coordinates

Table 3: GSA Ancillary static input files

3.3 Atmospheric and surface radiative transfer functions

Radiative transfer calculations have been performed for various surface and atmospheric conditions in order to obtain the pre-computed functions required to solve the inverse problem. Detailed information about the theoretical background justifying the use of these radiation transfer functions is provided in Section 3.6 . The values of these functions are given for discrete values of aerosol optical depth and for discrete values of the two parameters (k and Θ) characterizing the shape of the surface Bi-directional Reflectance Factor (BRF).

Given the specification of the Meteosat visible channel and the operational constraints in terms of memory and storage capacity, the radiation transfer problem has been segmented into two major parts: the absorption effect and scattering effect. The atmosphere is idealized as a multi-layer horizontally homogeneous system for which plane-parallel scattering theory is applicable. The organization of the layers follows the approach used in the 6S code (Vermote et al., 1997 [RD 32]). The gaseous absorption is assumed to take place on top of a scattering layer. All vertical profiles of the various atmospheric com-pounds correspond to those implemented in the 6S code. The Meteosat Surface Albedo algorithm uses the US-62 [RD 31] atmosphere specification as a default option. US-62 is the U.S. Standard atmospheric profile 1962.

The function values stored in the pre-Computed Radiation transfer Functions (CRAF) database are required to simulate the Meteosat BRF values for various aerosol optical depths and surface anisotropy conditions. These functions allow a simulation of the Meteosat signal using an approach where the contribution due to the coupled surface-aerosol scattering effects is calculated during the retrieval process. All the function values are weighted with the Meteosat spectral response.

The contribution to the Meteosat BRF values which is due to ozone and water vapour absorption effects is treated as a separate problem from scattering. This contribution is technically accounted for in the scattering module (ASM) via a simple division of the measured BRF values by the appropriate transmission factors due to the absorbing gases.

3.4 Description of the Data Accumulation Module (DAM)

To constrain the inverse radiation transfer problem and to limit the number of acceptable solutions that can account for the Meteosat data, we propose to exploit the high temporal sampling of the TOA BRF fields over a period of one day as if it were an instantaneous angular sampling with respect to the solar zenith angle. This is valid only assuming that the surface-atmosphere geophysical system does not change significantly during the period of data accumulation. A daily accumulation period corresponding to a number of images (NSLOT). A value of 25 is chosen as the default option for the module. For Meteosat, this encloses a period of 12 hours. The DAM stores, for all land pixels, a time series of ToA BRF with the following constraints:

- Pixel Sun zenith angle < 70°;
- Pixel ToA BRF between 0.05° and 0.6°

3.5 Description of the Data Consistency Procedure (DCP)

The Data Consistency Procedure (DCP) is applied for all pixels of the TOA BRF time series that has satisfied the previous DAM series of screening tests. In order to be interpreted by the physical modules at a later stage, the DCP checks the consistency of the retained BRF values by attempting to fit the data series against a general parametric BRF model, namely a modified version of the Rahman-Pinty-Verstraete (RPV) model, named MRPV (Engelsen et al. 1996 [RD 5]):

$$R_M(\theta_0, \theta, \phi; R_0, b_M, k_M) = R_0 M_I(\theta_0, \theta, k_M) F_M(g; b_M) H(\overline{R_{Msat}}, G)$$ *Equation 1*

The Minnaert function is defined:

$$M_I(\theta_0, \theta, k_M) = \frac{\cos^{k_M-1}\theta_0 \cos^{k_M-1}\theta}{(\cos\theta_0 + \cos\theta)^{1-k_M}}$$ *Equation 2*

The Henyey-Greenstein function is defined as:

$$F_M(g; b_M) = \exp(-b_M \cos g)$$ *Equation 3*

The Hot-spot function is defined as:

$$H(\overline{R_{Msat}}, G) = 1 + \frac{1 - \overline{R_{Msat}}}{1 + G}$$ *Equation 4*

The phase angle g is defined as:

$$\cos g = \cos\theta \cos\theta_0 + \sin\theta \sin\theta_0 \cos\phi$$ *Equation 5*

And the geometric factor G as follows:

$$G = [\tan^2\theta_0 + \tan^2\theta - 2\tan\theta_0\tan\theta\cos\phi]^{1/2} \quad \textit{Equation 6}$$

$R_{Msat,}$ is the average of the available measured reflectance factors, and where θ and θ_0 are the observation and illumination zenith angles respectively. The relative azimuth angle, φ, is zero when the source of illumination is behind the satellite.

Optimal model parameter values can then be found by application of a fast linear scheme since the hotspot factor $H(\overline{R_{Msat,}}\, G)$ (Equation 4) acts like a constant term in the model. See Engelsen et al. 1996 [RD 5]).

The optimization scheme is indeed applied to an expression of the type:

$$\ln\frac{R_M}{H(\overline{R_{Msat,}}\, G)} = \ln R_0 + (k_M - 1)\ln[\cos\theta_0\cos\theta(\cos\theta_0 + \cos\theta)] - b_M\cos g \quad \textit{Equation 7}$$

And the root mean square of the fit is estimated. The optimal coefficient values, namely R_0, b_M and k_M, are found by the application of a Cramer's Rule for solving of linear equations using determinants.

The DCP then compares the values of the standard deviation of the fit, against a pre-defined threshold value, which represents the maximum value of the standard deviation of the fit that is considered acceptable for successful interpretability. When the value of the fit below the threshold value, then the process escapes from the DSM and enters the ASM; otherwise, the observed BRF value exhibiting the largest absolute departure with respect to the model prediction is eliminated and the series of observed BRF values is screened again. This iteration procedure is pursued until an acceptable fit is obtained or when the remaining number of BRF data points in the time series becomes too low. In practice, the DCP estimates the following x^2_{DCP} function:

$$\chi^2_{DCP}(z_{sat}; R_0, k_M, b_M) = \frac{\sum_i [R_{Msat}(z_{sat}, i) - R_M(z_{sat}, i; R_0, k_M, b_M)]^2}{\sum_i \sigma^2_{DCP}(i)} \quad \textit{Equation 8}$$

where $R_{Msat}(z_{sat}, i)$ is the TOA BRF value measured at level Z_{sat} by Meteosat at the current slot i, $R_M(z_{sat}\, i; R_0, k_M, b_M)$ is the TOA BRF value simulated with the MRPV model for the same slot i using the optimal parameter values retrieved as indicated above, and $\sigma_{DCP}(i)$ is the maximum acceptable standard deviation value to guarantee an appro-priate smoothness and angular consistency between the reflectance in the various slots of the same day. This smoothness condition is ensured when $x^2_{DCP} \leq 1$.

The default option of the DCP uses a threshold value of six for the number of required BRF data points. Given the computational constraints, it is not envisaged to implement more complicated schemes as would be required to ensure that an optimal angular sampling is available.

The default $\sigma_{DCP}(i)$ value is equal to 10 % of the average value of the measured TOA BRFs, $R_{Msat}(z_{sat}, i)$ for a given Meteosat pixel. A value of 1.0 for the smoothness indicator namely x^2_{DCP} is assumed appropriate to ensure an adequate data smoothness.

The largest (lowest) values allowed for the parameters k_M and b_M are set at 1.2 (0.0) and 1.2 (–1.2), respectively, by default in the DCP. A flag value will be issued by the DCP to document the output according to the following events:

- Number of remaining BRF data points are less than six;
- More than six BRF data points are left but the values of the k_M and b_M model parameters falls outside the range of allowed values, and
- A successful pass of this fine-screening procedure.

The optimized values of the MRPV, R_0, k_M and b_M, will be archived for all terrestrial pixels, together with the squared value of the σ_{act} value, the value of x^2_{DCP}, the number of retained slots (NESC): and the number of slots removed by the DCP (NREM). All these products are generated daily for all processed pixels.

3.6 Description of the Atmospheric Scattering Module (ASM)

The albedo of a land surface is the non-dimensional ratio of the radiation flux reflected by a (typically horizontal) surface in all directions and the incoming irradiance, which is the radiation flux from the upper hemisphere. According to the inclusion or removal of the atmospheric scattering signal the radiation fluxes produce Bi-Hemispherical Reflectance (BHR) or Directional Hemispherical Reflectance (DHR), respectively (Pinty et al. 2005 [RD 25]). If the radiation impacting the surface can be assumed isotropic the BHR becomes BHR_{iso}, a quantity independent of ambient conditions. The BHR is commonly called blue sky albedo, while the DHR and BHR_{iso} are respectively called white and black sky albedo (Schaaf et al. 2002 [RD 29]). The relation between the BHR, DHR and BHR_{iso} can be expressed as follows: See Pinty et al. 2005 [RD 25]:

$$\mathrm{BHR}^*(z_0, \mu_0; \tau, \rho_{\mathrm{sfc}}) = \mathrm{DHR}(z_0, \mu_0; \rho_{\mathrm{sfc}}) f^{\downarrow \mathrm{dir}}(z_0, \mu_0; \tau) + \mathrm{BHR}_{\mathrm{iso}}(z_0; \rho_{\mathrm{sfc}}) f^{\downarrow \mathrm{diff}}(z_0, \mu_0; \tau, \rho_{\mathrm{sfc}}),$$

Equation 9

The fractions of diffuse and direct radiation are defined as:

$$f^{\downarrow \mathrm{diff}}(z_0, \mu_0; \tau, \rho_{\mathrm{sfc}}) = 1 - f^{\downarrow \mathrm{dir}}(z_0, \mu_0; \tau) = \frac{\pi [T_{\mathrm{iso}}(z_0, \mu_0; \tau) + T_{\mathrm{ms}}(z_0, \mu_0; \tau, \rho_{\mathrm{sfc}})]}{t^{\downarrow \mathrm{tot}}(z_0, \mu_0; \tau, \rho_{\mathrm{sfc}})},$$

Equation 10

The BHR_{iso} is defined as:

$$BHR_{iso} = \rho_0 \alpha_0$$

Equation 11

The ad hoc parameter α_0 is defined in Equation 46 (see Section 3.6.2) and ρ_0 is the amplitude of the Bidirectional Reflectance Factor (BRF) field. The DHR is defined in Equation 16 in Section 3.6.1).

3.6.1 Physics of the Problem

This section describes the core of the Surface Albedo algorithm and presents the physical and mathematical aspects of the atmospheric absorption and scattering problems when using Meteosat BRF data. Note that all physical variables appearing within a spectral integral are monochromatic quantities.

The equations required to solve the inverse problem and retrieve simultaneously the surface BRF field and the aerosol optical depth are described in the next section. The retrieval of surface quantities such as albedo values requires addressing the complex issue of specifying the lower boundary conditions of an atmospheric radiation transfer problem. Although many different related concepts can be used, the albedo, as a generic quantity, is required in applications dealing with land surface energy budget. The various definitions that can be used express different levels of assumptions made on the calculation of the surface quantities with respect to the angular integration of the incoming solar radiation. See Nicodemus et al. 1977 [RD 20].

Fundamentally, the basic physical quantity required by any kind of surface application is the Bidirectional Reflectance Factor (BRF). Indeed, this quantity expresses the probability for radiation coming from one specific direction, Ω', to be scattered into another specific direction, Ω, normalized by the same reflectance due to a Lambertian target. Accordingly, the upwelling radiance field at the surface level z_0 in the direction Ω, $I^{\uparrow}(z_0, \Omega, \Omega_0)$ can be expressed as follows:

$$I^{\uparrow}(z_0, \Omega, \Omega_0) = \frac{1}{\pi} \int_{2\pi} \rho_{sfc}(z_0, \Omega' \rightarrow \Omega)\, I^{\downarrow}(z_0, \Omega', \Omega_0)\, \mu'\, d\Omega' \qquad \textit{Equation 12}$$

where:

$\rho_{sfc}(z_0, \Omega' \rightarrow \Omega)$	represents the Bi-directional Reflectance Factor of the surface
$I^{\downarrow}(z_0, \Omega', \Omega_0)$	is the downwelling radiance in the direction Ω' at the bottom of the atmosphere which is generated when the Sun is illuminating from the direction Ω_0

All physical quantities intervening in Equation 12 are monochromatic spectral quantities. Since radiant exitance quantities, rather than radiances, are desirable for most applications involving a surface energy budget equation, it is necessary to compute the integral of $I^{\uparrow}(z_0, \Omega, \Omega_0)$ over all exiting directions Ω in the upward-looking hemisphere:

$$E^{\uparrow}(z_0, \mu_0) = \int_{2\pi} I^{\uparrow}(z_0, \Omega, \Omega_0)\, \mu\, d\Omega \qquad \textit{Equation 13}$$

where μ_0 is the cosine of the solar zenith angle.

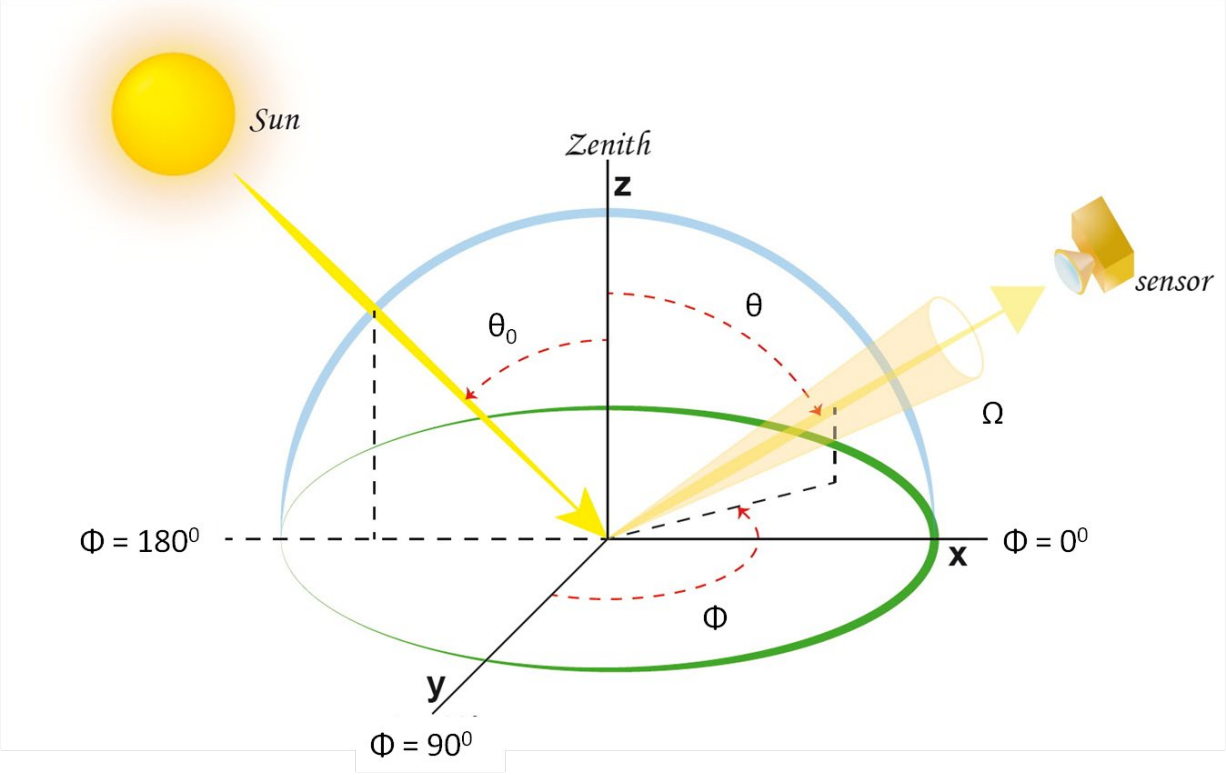

Figure 6: Schematic diagram showing angles used in the definition of BRF and albedo (θ: zenith angle; Φ: azimuth angle; i: incident; r: reflected; ω: solid angle). ***Note****: Graphic is based from a picture taken in the Global Albedo Project webpage:* See **http://www-c4.ucsd.edu/gap/**

Similarly, the non-isotropic downwelling radiance field can be integrated over all incoming directions in the downward looking hemisphere, to estimate the surface irradiance as follows:

$$E^{\downarrow}(z_0;\mu_0) = \int_{2\pi} I^{\downarrow}(z_0,\Omega',\Omega_0)\,\mu'\,d\Omega' \qquad \textit{Equation 14}$$

and the BiHemispherical Reflectance (BHR) is obtained by forming the ratio of the radiant exitance to surface irradiance, namely the ratio of Equation 13 to Equation 14:

$$BHR(z_0,\mu_0) = \frac{E^{\uparrow}(z_0;\mu_0)}{E^{\downarrow}(z_0;\mu_0)} \qquad \textit{Equation 15}$$

BHR values are controlled jointly by surface and atmospheric properties. Depending on accuracy requirements and the context of the application, other quantities can easily be derived from Equation 10 and Equation 11. For instance, the Directional-Hemispherical Reflectance (DHR) can be obtained by separating the direct and diffuse components of the downwelling radiance field. When considering direct radiation only, the DHR can then be written as follows:

$$DHR(z_0,\mu_0) = \frac{1}{\pi}\int_{2\pi} \rho_{sfc}(z_0,\Omega' \rightarrow \Omega)\mu' d\,\Omega' \qquad \textit{Equation 16}$$

Since the direct solar illumination is depending only on Ω_0, it is equal to zero for all Ω' directions except the particular Ω_0 direction. Analogous albedo values could be derived with respect to the

atmospherically diffuse component, with or without the assumptions of isotropic downwelling sky radiance fields. The geometry of the retrieval is represented in Figure 6.

3.6.2 Mathematical Implementation of the Algorithm

The radiance measured by Meteosat is controlled by all radiative processes which represent how the solar radiation has interacted with the coupled surface-atmosphere system. Accordingly, Meteosat radiances depend on a large number of state variables characterizing both atmospheric and surface absorbing and scattering properties.

The radiance measured by the satellite can be decomposed as a sum of terms, one of which constitutes the contribution specifically due to surface scattering effects, which will be used to derive the surface albedo products:

$$I^{\Uparrow}_{Msat}(z_{sat}, \Omega, \Omega_0) = \int_{\lambda_1}^{\lambda_2} I^{\Uparrow}_{atm}(z_{sat}, \Omega, \Omega_0)\, S(\lambda)\, d\lambda + \int_{\lambda_1}^{\lambda_2} I^{\Uparrow}_{sfc}(z_{sat}, \Omega, \Omega_0)\, S(\lambda)\, d\lambda$$

Equation 17

where $I^{\Uparrow}_{Msat}$ (z_{sat}, Ω, Ω_0) denotes the radiance measured at the altitude of the satellite (z_{sat}) by the Meteosat sensor, observing in direction Ω, integrated between the lower and upper limits (λ_1 and λ_2, respectively) of the Meteosat spectral response denoted $S(\lambda)$. The above expression is appropriate for isolating the contribution due to the radiation that has not interacted with the surface but only with the atmosphere, $I^{\Uparrow}_{atm}$ (z_{sat}, Ω, Ω_0).

The surface spectral radiance contribution, including absorption and scattering effects, $I^{\Uparrow}_{sfc}$ (z_{sat}, Ω, Ω_0), is related to the surface scattering properties as follows:

$$I^{\Uparrow}_{sfc}(z_{sat}, \Omega, \Omega_0) = \frac{1}{\pi} \int_0^1 \int_{2\pi} \int_0^1 \int_{2\pi} \rho_{sfc}(z_0, \Omega' \rightarrow \Omega'') I^{\downarrow}(z_0, \Omega', \Omega_0) \times T^{\Uparrow}(\Omega'', \Omega)\, \mu'\, d\Omega'\, \mu''\, d\Omega''$$

Equation 18

where $T^{\Uparrow}(\Omega'', \Omega)$ represents the total spectral atmospheric transmission factor in direction Ω of the surface upwelling radiance field in the direction Ω''. The latter is generated by the scattering in direction Ω of the downwelling radiance field at the surface level z_0. In Equation 18, $\rho_{sfc}(z_0, \Omega' \rightarrow \Omega'')$ corresponds to the BRF of the surface which is the basic quantity required to estimate the surface albedo.

The retrieval of surface albedo values therefore consists in developing an inverse procedure allowing the separation between the radiative properties of the atmosphere and the surface. Appropriate models exist for evaluating the radiation regime in a coupled surface-atmosphere system and then deduce the relevant scattering functions and associated radiance fields. It is then feasible to pre-compute and store in Look-Up Tables (LUTs) a large number of such functions and radiance fields generated in a forward mode for an extensive set of pre-defined geophysical situations. Obviously, such a set must cover a large range of geophysical situations and it would request a calculation power hardly reachable in a standard operational reprocessing system. The two easiest ways to reduce the

computational load consist of limiting the number of retrieved parameters and introducing a few *ad hoc* physical and mathematical simplifications on the problem to be solved.

The Surface Albedo algorithm takes advantage of the routine availability of data on atmospheric fields of ozone and water vapor content to reduce the inverse problem to a scattering problem only. It further assumes that only a finite set of pre-defined types of atmospheres can be considered and that atmospheric functions and radiance fields can be pre-computed for discrete values of the aerosol optical depth and black surface conditions. To limit the number of entries of the LUTs and the size of the CRAF database, the algorithm implements a simplified atmospheric model where the gas absorbing layers are located on top of the scattering layers; this scheme is similar to the one adopted in the 6S code (Vermote et al. 1997 [RD 32]).

The radiance measured by the Meteosat sensor Equation 17 can then be rewritten as follows:

$$I^{\Uparrow}_{Msat}(z_{sat},\Omega,\Omega_0) = \int_{\lambda_1}^{\lambda_2} T^{gas}(\Omega,\Omega_0)\, I^{\uparrow}_{atm}(z_{soa},\Omega,\Omega_0)\, S(\lambda)\, d\lambda + \int_{\lambda_1}^{\lambda_2} T^{gas}(\Omega,\Omega_0)\, I^{\uparrow}_{sfc}(z_{soa},\Omega,\Omega_0)\, S(\lambda)\, d\lambda$$

Equation 19

where:

$I^{\uparrow}_{atm}$ (z_{soa}, Ω, Ω$_0$)	represents spectral radiance values due to scattering effects only, –emerging from the top of a Scattering-Only-Atmosphere identified by the level z_{soa},
$I^{\uparrow}_{sfc}$ (z_{soa}, Ω, Ω$_0$)	represents spectral radiance values due to scattering effects only, –emerging from the top of a Scattering-Only-Atmosphere identified by the level z_{soa},
T^{gas} (Ω, Ω$_0$)	denotes the spectral transmission factor due to gaseous absorption effects, primarily controlled by ozone and water vapour.

Equation 19 shows that the radiance fields due to the atmosphere and the surface must be computed as a function of the actual amounts of absorbing gases. To fully separate the absorption and scattering effects, Equation 19 was modified as follows:

$$I^{\Uparrow}_{Msat}(z_{sat},\Omega,\Omega_0) = T^{gas}_{Msat}(U_{O_3},U_{H_2O},\Omega,\Omega_0)\left[\tilde{I}^{\uparrow}_{atm}(z_{soa},\Omega,\Omega_0) + \tilde{I}^{\uparrow}_{sfc}(z_{soa},\Omega,\Omega_0)\right]$$

Equation 20

T^{gas}_{Msat} (U_{O_3}, U_{H_2O}, Ω, Ω$_0$) denotes the transmission factor due to gaseous absorption (ozone U_{O_3} and UH2O water vapour), weighted by the spectral response of the Meteosat sensor and it is defined:

$$T^{gas}_{Msat}(U_{O_3},U_{H_2O},\Omega,\Omega_0) = \frac{\int_{\lambda_1}^{\lambda_2} E_0(\theta_0)\, T^{gas}(\Omega,\Omega_0)\, S(\lambda)\, d\lambda}{\int_{\lambda_1}^{\lambda_2} E_0(\theta_0)\, S(\lambda)\, d\lambda}$$

Equation 21

where $E_0(\theta_0)$ is the spectral extra-terrestrial solar irradiance.

For the sake of consistency, the scattered radiance fields emerging at the top of the Scattering-Only-Atmosphere and weighted by the Meteosat spectral response are then approximated as follows:

$$\tilde{I}^{\uparrow}_{atm}(z_{soa},\Omega,\Omega_0)=\frac{\int_{\lambda_1}^{\lambda_2}E_0(\theta_0)\,T^{gas}(\Omega,\Omega_0)\,I^{\uparrow}_{atm}(z_{soa},\Omega,\Omega_0)\,S(\lambda)\,d\lambda}{\int_{\lambda_1}^{\lambda_2}E_0(\theta_0)\,T^{gas}(\Omega,\Omega_0)\,S(\lambda)\,d\lambda}\int_{\lambda_1}^{\lambda_2}S(\lambda)\,d\lambda$$

Equation 22

and,

$$\tilde{I}^{\uparrow}_{sfc}(z_{soa},\Omega,\Omega_0)=\frac{\int_{\lambda_1}^{\lambda_2}E_0(\theta_0)\,T^{gas}(\Omega,\Omega_0)\,I^{\uparrow}_{sfc}(z_{soa},\Omega,\Omega_0)\,S(\lambda)\,d\lambda}{\int_{\lambda_1}^{\lambda_2}E_0(\theta_0)\,T^{gas}(\Omega,\Omega_0)\,S(\lambda)\,d\lambda}\int_{\lambda_1}^{\lambda_2}S(\lambda)\,d\lambda$$

Equation 23

In the current implementation, the integral in the denominators of Equation 22 and Equation 23 are approximated using fixed values for the ozone ($\overline{U_{O_3}}$) and water vapour amount ($\overline{U_{H_2O}}$), so that the computation is done once and yields a constant value. See the error values on the computation of the exact transmission factor over the Meteosat channel which is associated with this latter approximation remain less than 3 %, even when considering extreme angular conditions and gas amounts.

All dimensionless factors related to BRF and transmission quantities which are required to represent the scattering regime between the surface and the atmosphere over the Meteosat spectral band will be approximated by the following generic formulation:

$$\tilde{Y}=\frac{\int_{\lambda_1}^{\lambda_2}E_0(\theta_0)\,T^{gas}(\overline{U_{O_3}},\overline{U_{H_2O}},\Omega,\Omega_0)\,Y\,S(\lambda)\,d\lambda}{\int_{\lambda_1}^{\lambda_2}E_0(\theta_0)\,T^{gas}(\overline{U_{O_3}},\overline{U_{H_2O}},\Omega,\Omega_0)\,S(\lambda)\,d\lambda}$$

Equation 24

where *Y* represents any one of the spectral atmospheric scattering functions or parameters controlling the radiation transfer processes between the Sun, the surface and the satellite.

The above physical assumptions and mathematical approximations allow a major step forward in the interpretation of Meteosat BRF data to retrieve surface albedo quantities. Indeed, the problem now reduces to the correct representation and modelling of a surface atmosphere scattering situation. Furthermore, the surface-atmosphere scattering problem can then be addressed spectrally since Equation 24 permits only to approximate the values of scattering functions and parameters, weighted by the Meteosat spectral response, from their monochromatic values.

Since all atmospheric properties and functions can be derived and pre-computed off-line, the only remaining issue concerns the use of an appropriate model to represent the surface BRF field, $\rho_{sfc}(z_0, \Omega' \rightarrow \Omega)$. This model must have enough flexibility to be applicable over a wide range of surface types, conditions and wavelengths, but it must also be as simple as possible to limit the computational cost involved in estimating Equation 17.

The RPV model published by Rahman et al. (1993) [RD 28], developed with similar requirements and extensively tested (see Privette et al. 1997 [RD 27], Cabot and Dedieu 1997 [RD 2], and Engelsen et al. 1996 [RD 5]) has been selected here for this purpose:

$$\rho_{sfc}(z_0,\Omega_0\rightarrow\Omega;\rho_0,\rho_c,\Theta,k)=\rho_0\,\breve{\rho}_{sfc}(z_0,\Omega_0\rightarrow\Omega;\rho_c,\Theta,k)$$

Equation 25

where:

ρ_0 and $\check{\rho}_{sfc}(z_0, \Omega_0 \rightarrow \Omega; \rho_c, \Theta, k)$	describes the amplitude and the angular field of the surface BRF

This latter quantity is expressed by the following equation:

$$\check{\rho}_{sfc}(z_0, \Omega_0 \rightarrow \Omega; \rho_c, \Theta, k) = M_I(\theta_0, \theta; k)\, F_{HG}(g; \Theta_{HG})\, H(\rho_c; G) \qquad \textit{Equation 26}$$

Each parameter only appears in one single factor as defined in the following three equations:

$$M_I(\theta_0, \theta; k) = \frac{\cos^{k-1}\theta_0 \cos^{k-1}\theta}{(\cos\theta_0 + \cos\theta)^{1-k}} \qquad \textit{Equation 27}$$

$$F_{HG}(g; \Theta_{HG}) = \frac{1 - \Theta_{HG}^2}{[1 + 2\Theta_{HG}\cos g + \Theta_{HG}^2]^{3/2}} \qquad \textit{Equation 28}$$

$$H(\rho_c; G) = 1 + \frac{1 - \rho_c}{1 + G} \qquad \textit{Equation 29}$$

One major advantage of the RPV model is that the parameter which mainly controls the estimation of surface albedo values, namely the amplitude of the BRF, appears as a factor in a product of three decoupled angular functions (M, F, and H). A graphical interpretation of the parameters controlling the three angular functions is given in Figure 7: RPV model parameters

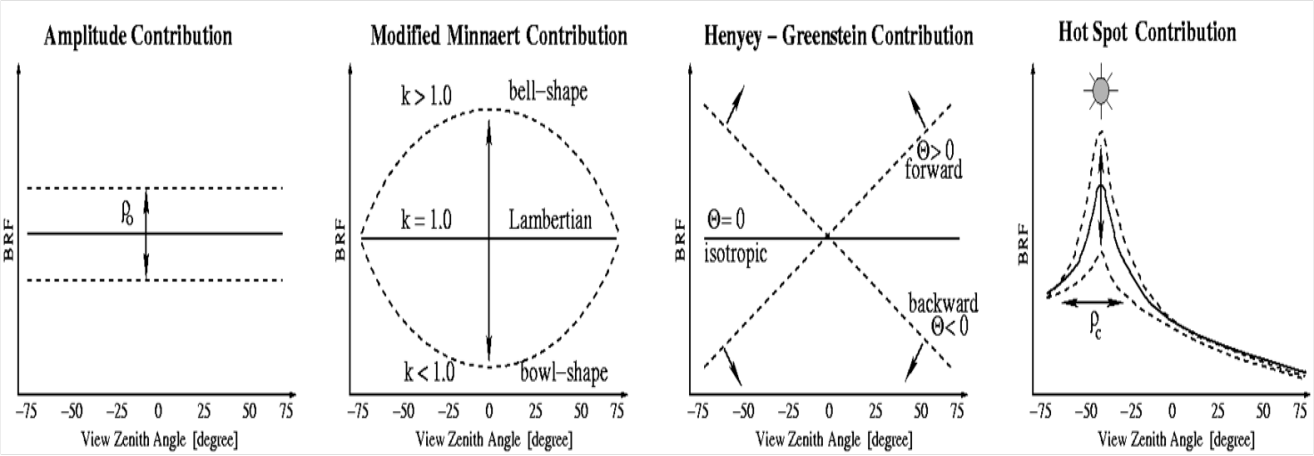

Figure 7: RPV model parameters

Since the calculation of the surface radiance contribution (see Equation 18) requires the estimation of a set of integrals over angular coordinates, it is appropriate to factor out this first parameter in the expression describing the surface spectral radiance contribution due to scattering effects only:

$$I^{\uparrow}_{sfc}(z_{soa},\Omega,\Omega_0) = \frac{\rho_0}{\pi}\int_0^1\int_{2\pi}\int_0^1\int_{2\pi}\breve{\rho}_{sfc}(z_0,\Omega'\rightarrow\Omega'';\rho_c,\Theta,k) \times I^{\downarrow}_{sfc}(z_0,\Omega',\Omega_0)T^{\uparrow}(\Omega'',\Omega)\,\mu'\,d\Omega'\,\mu''\,d\Omega''$$

Equation 30

where $I^{\downarrow}_{sfc}(z_0, \Omega', \Omega_0)$ corresponds to the downwelling spectral radiance reaching the surface and $T^{\uparrow}(\Omega'', \Omega)$ represents the spectral atmospheric transmission factor in direction Ω of the upwelling radiance field scattered by the surface in direction Ω''.

In the following, the functions and factors applied to characterize the origin and direction of the radiation are identified by negative (positive) values of the cosine of the zenith angles (μ) for upward (downward) travelling directions. To limit the computational cost of the algorithm, additional developments follow the strategy proposed by Diner et al. (1997) [RD 4] and Martonchik et al. (1998) [RD 5], both sides of Equation 30 are multiplied by the factor $\pi / E_0\mu_0$ to transform all upwelling radiance quantities into BRFs and downwelling radiance quantities into transmittance factors:

$$\rho_{sfc}(z_{soa},\Omega_0\rightarrow\Omega) = \frac{I^{\uparrow}_{sfc}(z_{soa},\Omega,\Omega_0)\,\pi}{E_0\,\mu_0}$$

Equation 31

and

$$T^{\downarrow}(\Omega',\Omega_0) = \frac{I^{\downarrow}_{sfc}(z_0,\Omega',\Omega_0)\,\pi}{E_0\,\mu_0}$$

Equation 32

The ρ_c value controlling the hot spot function in $\breve{\rho}_{sfc}(z_0, \Omega' \rightarrow \Omega; \rho_c, \Theta_{HG}, k)$ is fixed at a value equal to 0.15. The functions $T^{\downarrow}(\Omega', \Omega_0)$ and $T^{\uparrow}(\Omega'', \Omega)$ in Equation 30 are expanded to separate the direct and diffuse contributions to the total signal for both upward and downward fields:

$$T^{\downarrow}(z_0, \Omega', \Omega_0) = \exp(-\tau/\mu_0)\,\delta(\mu_0 - \mu)\,\delta(\phi_0 - \phi) + T(\mu_0, \mu, \phi_0 - \phi) \quad \textit{Equation 33}$$

for the downward solar radiation, and

$$T^{\uparrow}(z_0, \Omega, \Omega') = \exp(-\tau/|\mu|)\,\delta(|\mu| - |\mu'|)\,\delta(\phi - \phi') + T(-\mu, -\mu', \phi - \phi') \quad \textit{Equation 34}$$

for the upward solar radiation.

The scattering functions and the diffuse transmittance factors which depend on the difference between two azimuth angles, $T(\mu_0, \mu, \varphi_0 - \varphi)$, $T(-\mu, -\mu', \varphi - \varphi')$ and $\breve{\rho}_{sfc}(z_0, \Omega' \rightarrow \Omega; \rho_c, \Theta_{HG}, k)$ are expanded as cosine Fourier series with respect to the relative azimuth angle. The reciprocity principle applies to both upward and downward diffuse transmittance factors, $T(\mu, \mu', \varphi - \varphi') = T(-\mu', -\mu, \varphi' - \varphi)$.

With the Fourier expansion, the transmission factors for diffuse radiation become:

$$T(\mu_0, \mu, \phi_0 - \phi) = T_0(\mu_0, \mu) + T_1(\mu_0, \mu)\,\cos(\phi_0 - \phi) \quad \textit{Equation 35}$$

for the downward radiation, and

$$T(-\mu, -\mu', \phi - \phi') = T_0(-\mu, -\mu') + T_1(-\mu, -\mu')\,\cos(\phi - \phi') \quad \textit{Equation 36}$$

for the upward radiation. Similarly, the $\breve{\rho}_{sfc}(z_0, \Omega' \rightarrow \Omega; \rho_c, \Theta_{HG}, k)$ function is approximated by (with omission of the dependent variables, ρ_c, Θ_{HG} and k):

$$\breve{\rho}_{sfc}(z_0, \mu_0, -\mu', \phi_0 - \phi') = r_0(\mu_0, -\mu') + r_1(\mu_0, -\mu')\,\cos(\phi_0 - \phi') \quad \textit{Equation 37}$$

when the diffuse transmission in the upward direction of the direct solar radiation scattered by the surface is considered, and:

$$\breve{\rho}_{sfc}(z_0, \mu', -\mu, \phi' - \phi) = r_0(\mu', -\mu) + r_1(\mu', -\mu)\,\cos(\phi' - \phi) \quad \textit{Equation 38}$$

when the scattering by the surface of downward diffuse solar radiation is considered. In Equation 35 to Equation 38, the coefficients noted with an index 0 and 1 represent the first two Fourier coefficients, that is:

$$Y(\mu', -\mu, \phi' - \phi) = Y_0(\mu', -\mu) + Y_1(\mu', -\mu)\,\cos(\phi' - \phi) \quad \textit{Equation 39}$$

with:

$$Y_0(\mu', -\mu) = \frac{1}{2\pi} \int_0^{2\pi} Y(\mu', -\mu, \phi' - \phi)\, d\phi' \qquad \textit{Equation 40}$$

and

$$Y_1(\mu', -\mu) = \frac{1}{\pi} \int_0^{2\pi} Y(\mu', -\mu, \phi' - \phi)\, \cos(\phi' - \phi)\, d\phi' \qquad \textit{Equation 41}$$

Using Equation 29, Equation 28 can be reformulated as follows:

$$\rho_{sfc}(z_{soa}, -\mu, \mu_0, \phi - \phi_0) = \rho_0\, \check{\rho}_{sfc}(z_{soa}, -\mu, \mu_0, \phi - \phi_0) \qquad \textit{Equation 42}$$

where $\check{\rho}_{sfc}\,(z_{soa}, -\mu, \mu_0, \varphi - \varphi_0)$ represents the angular field of the spectral bidirectional reflectance factor at the top of the scattering-only atmosphere. By separating the direct and diffuse contributions to the transmission factors for upward and downward radiation, this latter factor can be expressed as follows:

$$\begin{aligned}
&\check{\rho}_{sfc}(z_{soa}, -\mu, \mu_0, \phi - \phi_0) = \\
&\quad \exp(-\tau/\mu_0)\, \exp(-\tau/|\mu|)\, \check{\rho}_{sfc}(z_0, \Omega_0 \to \Omega; \rho_c, \Theta_{HG}, k) \\
&\quad + \exp(-\tau/|\mu|) \int_0^{2\pi} \int_0^1 T(\mu_0, \mu', \phi_0 - \phi')\, \check{\rho}_{sfc}(z_0, \mu', -\mu, \phi' - \phi)\, \mu'\, d\mu'\, d\phi' \\
&\quad + \exp(-\tau/\mu_0) \int_0^{2\pi} \int_0^1 T(-\mu, -\mu', \phi - \phi')\, \check{\rho}_{sfc}(z_0, \mu_0, -\mu', \phi_0 - \phi')\, \mu'\, d\mu'\, d\phi' \\
&\quad + \int_0^{2\pi} \int_0^1 \int_0^{2\pi} \int_0^1 T(\mu_0, \mu', \phi_0 - \phi')\, \check{\rho}_{sfc}(z_0, \mu', -\mu'', \phi' - \phi'') \\
&\quad \times T(-\mu, -\mu'', \phi - \phi'')\, \mu'\, d\mu'\, d\phi'\, \mu''\, d\mu''\, d\phi''
\end{aligned} \qquad \textit{Equation 43}$$

Since the Fourier expansion is used only when diffuse transmission factors for upward and downward radiation are considered, the following generic equation can be derived to express the angular field of the spectral bidirectional reflectance factor at the top of the scattering-only atmosphere:

$$\begin{aligned}
\check{\rho}_{sfc}(z_{soa}, -\mu, \mu_0, \phi - \phi_0) &= \exp(-\tau/\mu_0)\, \exp(-\tau/|\mu|)\, \check{\rho}_{sfc}(z_0, \Omega_0 \to \Omega; \rho_c, \Theta_{HG}, k) \\
&+ \exp(-\tau/|\mu|)\, [f_0(\mu_0, -\mu) + f_1(\mu_0, -\mu)\, \cos(\phi_0 - \phi)] \\
&+ \exp(-\tau/\mu_0)\, [g_0(-\mu, \mu_0) + g_1(-\mu, \mu_0)\, \cos(\phi_0 - \phi)] \\
&+ [h_0(-\mu, \mu_0) + h_1(-\mu, \mu_0)\, \cos(\phi_0 - \phi)] \\
&+ \rho^{ms}(-\mu, \mu_0)
\end{aligned} \qquad \textit{Equation 44}$$

where:

$$
\begin{aligned}
f_0(\mu_0,-\mu) &= 2\pi\int_0^1 T_0(\mu_0,\mu')\,r_0(\mu',\mu)\,\mu'\,d\mu' \\
f_1(\mu_0,-\mu) &= \pi\int_0^1 T_1(\mu_0,\mu')\,r_1(\mu',\mu)\,\mu'\,d\mu' \\
g_0(-\mu,\mu_0) &= 2\pi\int_0^1 T_0(-\mu,-\mu')\,r_0(\mu_0,-\mu')\,\mu'\,d\mu' \\
g_1(-\mu,\mu_0) &= \pi\int_0^1 T_1(-\mu,-\mu')\,r_1(\mu_0,-\mu')\,\mu'\,d\mu' \\
h_0(\mu_0,-\mu) &= 2\pi\int_0^1 T_0(-\mu'',-\mu)\,f_0(\mu_0,-\mu'')\,\mu''\,d\mu'' \\
h_1(\mu_0,-\mu) &= \pi\int_0^1 T_1(-\mu'',-\mu)\,f_1(\mu_0,-\mu'')\,\mu''\,d\mu''
\end{aligned}
$$

Equation 45

The right side of Equation 44 is composed of a sum of five terms representing the following contributions to the BRF at the top of the scattering-only-atmosphere, after multiplication by P_o . See also Equation 28:

Term 1	Direct downwelling radiation from direction Ω_0 scattered by the surface using the complete BRF model (Equation 25) and transmitted directly to the satellite in direction Ω.
Term 2	Diffuse incoming radiation scattered by the surface using the azimuthally averaged BRF model and reaching the top of the scattering-only-atmosphere after attenuation by the transmission factor for direct radiation.
Term 3	Direct incoming radiation scattered by the surface using the azimuthally averaged BRF model and reaching the top of the scattering-only-atmosphere after attenuation by the transmission factor for upward diffuse radiation.
Term 4	Diffuse incoming radiation scattered by the surface using the azimuthally averaged BRF model and then attenuated in the viewing direction of the satellite by the transmission factor for upward diffuse radiation.
Term 5	Total downwelling radiation scattered multiple times between the surface and the atmosphere, using the azimuthally averaged BRF model and the spherical albedo of the atmosphere, which reaches the top of the scattering-only-atmosphere after attenuation by the transmission factor for total upward radiation.

The fifth term of Equation 44, noted $\rho^{ms}(-\mu, \mu_0)$, corresponds to the contribution due to multiple scattering events between the surface and the lower atmosphere. This contribution is the most difficult one to express when bidirectional scattering properties of the two media are considered. However, since the intrinsic reflectance of the surface and the lower atmosphere illuminated from below take low values in the Meteosat spectral range, it is accurate enough to estimate this contribution using angularly averaged scattering properties both for the surface and for the atmosphere. In practice, this additional source of surface radiation can be described by an infinite sum of terms which can then be approximated by a geometrical series (see Lenoble, 1985 [RD 16]).

The angularly-averaged scattering property of the bottom of the atmosphere is a Bi-Hemispherical albedo, *S*, estimated in atmospheric radiation transfer models. See Vermote et al., 1997 [RD 32]. For the surface, the following *ad hoc* parameter, α_0, can be introduced:

$$\alpha_0 = 4 \int_0^1 \int_0^1 r_0(\mu', -\mu)\, \mu'\, d\mu'\, \mu\, d\mu$$ *Equation 46*

where $r_0(\mu', -\mu)$ is the first Fourier coefficient in Equation 38. Accordingly, the source term at the surface level which is due to multiple scattering between the surface and the atmosphere can be approximated by the following:

$$S^{ms}(\mu_0) = \frac{\alpha_0\, S}{1 - \rho_0\, \alpha_0\, S}\, \rho_0 \left[\exp(-\tau/\mu_0) + \overline{T}(\mu_0)\right]$$ *Equation 47*

with

$$\overline{T}(\mu_0) = \int_0^1 T_0(\mu_0, \mu)\, \mu\, d\mu$$ *Equation 48*

This source term can then be scattered by the surface and transmitted upward in the viewing direction of the satellite. This latter process can be parameterized as follows:

$$\rho^{ms}(-\mu, \mu_0) = S^{ms}(\mu_0)\, \left[\exp(-\tau/|\mu|)\, A(-\mu) + a(-\mu)\right]$$ *Equation 49*

with

$$A(-\mu) = 2 \int_0^1 r_0(-\mu, \mu')\, \mu'\, d\mu'$$ *Equation 50*

and

$$a(-\mu) = 2\pi \int_0^1 T_0(-\mu, \mu')\, A(-\mu')\, d\mu'$$ *Equation 51*

In an operational context, the costs associated with the computation of the integrals involved in Equation 45, Equation 50 and Equation 51, and all other atmospheric functions can be significantly reduced by pre-computing the values of these functions and storing them in LUTs. This, however, implies that a limited number of pre-defined solutions to the inverse problem will be considered, especially for the parameters *k* and Θ_{HG} controlling the shape of the surface BRF, for instance in all equations involving the $\breve{\rho}_{sfc}\,(z_0, \Omega' \rightarrow \Omega; \rho_c, \Theta_{HG}, k)$ function.

All the functions intervening in Equation 44 are computed on a monochromatic basis using the successive orders of scattering method implemented in the 6S code. See Vermote, *et al*. 1997 [RD 32].

aerosol optical depth @ 550 nm	0.1, 0.2, 0.3, 0.4, 0.6, 0.8, 1.0
k parameter (see Equation **26**)	0.4, 0.5, 0.6, 0.7, 0.8, 0.9, 1.0
Θ_{HG} parameter (see Equation **26**)	-0.30, -0.25, -0.20, -0.15, -0.10, -0.05, 0.00

Table 4: RTM model parameter discretization

These factors are computed for a predefined set of discrete values as shown in Table 4 and then weighted using Meteosat spectral response is estimated using Equation 24. The same procedure is applied to the exponential functions representing the transmission factors for direct radiation required in Equation 44, Equation 47, and Equation 49.

In summary, the following set of functions are pre-computed and stored in the CRAF database:

Function	***Found in***
T_{Msat}^{gas} (U_{O3}, U_{H2O}, Ω, Ω_0)	Equation 20
$I_{atm}^{\uparrow}$ (z_{sat}, Ω, Ω_0)	Equation 20
$\tilde{f}_0(\mu_0, -\mu)$	Equation 45
$\tilde{f}_1(\mu_0, -\mu)$	Equation 45
$\tilde{g}_0(-\mu, \mu_0)$	Equation 45
$\tilde{g}_1(-\mu, \mu_0)$	Equation 45
$\tilde{h}_0(\mu_0, -\mu)$	Equation 45
$\tilde{h}_1(\mu_0, -\mu)$	Equation 45
$\tilde{A}(-\mu)$	Equation 50
$\tilde{\alpha}(-\mu)$	Equation 51
$\tilde{T}(\mu_0)$	Equation 48
$\tilde{\alpha}^0$	Equation 46
S	Equation 47

Section 5 describes the input parameter values used to pre-compute these functions in the default version of the Surface Albedo algorithm using the US-62 atmosphere for sea-level conditions. The gaseous transmission functions for ozone and water vapour are pre-computed with the 6S code (Vermote *et al.* 1997 [RD 32]). The diffuse transmittance factors and all other aerosol related parameters and functions are pre-computed using the version of Successive Orders of Scattering which is implemented in the 6S code. All these expressions are evaluated on a standard grid of aerosol optical depths and use standard Gaussian quadrature points in μ and μ' . See Appendix Section B.2.

As indicated above, all computations were originally made on a monochromatic basis. Once these results are spectrally weighted (see Equation 24) to account for the particular spectral function of the Meteosat instrument, the model parameters ρ_0, k, and Θ_{HG} retrieved by the application of this algorithm to the Meteosat data yields 'effective' parameters which will be denoted $\tilde{\rho}_0$, $\tilde{k}$, and $\tilde{\Theta}_{HG}$, respectively. In other words, these values, as well as those derived from them, depend on the specific spectral response of the instrument. The values of the 'effective' parameters, therefore implicitly account for the effects due to the spectral changes of mostly all terrestrial surfaces within the Meteosat visible channel.

The mathematical developments proposed in this section can be summarized by the following transformation of the original Equation 20:

$$R_M(z_{sat}, -\mu, \mu_0, \phi - \phi_0; \tau, \tilde{\rho}_0, \tilde{k}, \tilde{\Theta}_{HG}) = T^{gas}_{Msat}(-\mu, \mu_0; U_{O_3}, U_{H_2O}) \times \left[\tilde{\rho}_{atm}(z_{soa}, -\mu, \mu_0, \phi - \phi_0; \tau) + \tilde{\rho}_0\, \tilde{\rho}_{sfc}(z_{soa}, -\mu, \mu_0, \phi - \phi_0; \tau, \tilde{\rho}_0, \tilde{\rho}_c, \tilde{k}, \tilde{\Theta}_{HG})\right] \quad \textit{Equation 52}$$

where:

$$R_M(z_{sat}, -\mu, \mu_0, \phi - \phi_0; U_{O_3}, U_{H_2O}, \tau, \tilde{\rho}_0, \tilde{k}, \tilde{\Theta}_{HG}) = \frac{I^{\Uparrow}_{Msat}(z_{sat}, \Omega, \Omega_0)\,\pi}{\mu_0 \int_{\lambda_1}^{\lambda_2} E_0(\theta_0)\, S(\lambda)\, d\lambda} \quad \textit{Equation 53}$$

and,

$$\tilde{\rho}_{atm}(z_{soa}, -\mu, \mu_0, \phi - \phi_0; \tau) = \frac{\tilde{I}^{\uparrow}_{atm}(z_{soa}, \Omega, \Omega_0)\,\pi}{\mu_0 \int_{\lambda_1}^{\lambda_2} E_0(\theta_0)\, S(\lambda)\, d\lambda} \quad \textit{Equation 54}$$

In Equation 54, $\tilde{\rho}_{atm}\,(z_{soa}, -\mu, \mu_0, \varphi - \varphi_0; \tau)$ represents the contribution, due to the intrinsic reflectance of the scattering-only-atmosphere, weighted by the Meteosat spectral response to the total BRF, namely $R_M(z_{sat}, -\mu, \mu_0, \varphi - \varphi_0; U_{O3}, U_{H2O}, \tau, \tilde{\rho}_0, \tilde{k}, \tilde{\Theta}_{HG})$.

This formulation summarizes the set of dependent and independent variables required to simulate the Meteosat observations under a variety of geophysical situations. The following mathematical manipulations have been applied:

- the decoupling between absorption and scattering processes;
- the quasi-linearization of Equation 20 with respect to the parameter describing the amplitude of the surface BRF ($\tilde{\rho}_0$);
- the expansion of scattered radiation as a Fourier series in relative azimuth angles and;
- the explicit contribution of atmospheric functions related to the radiation transfer regime for a black surface condition.

This strategy allows a straightforward implementation of the forward radiation transfer model since only sums and products of functions are required during the retrieval process. The Fourier expansion in $d\varphi$ values also avoids creating LUTs with an entry for this latter coordinate and, therefore, significantly reduces the memory size requirements of the processing.

The $\tilde{\rho}$ values are estimated, for all the pre-defined conditions of the surface-atmosphere scattering model based on the various values for the τ, $\tilde{k}$ and $\tilde{\Theta}_{HG}$ parameters, using the following equation:

$$\tilde{\rho}_0 = \frac{\sum_i W_{inv}(i)\ [R_{Msat}(z_{sat}, i)/T^{gas}_{Msat}(i; U_{O_3}, U_{H_2O}) - \tilde{\rho}_{atm}(z_{soa}, i; \tau)]}{\sum_i W_{inv}(i)\ \tilde{\rho}_{sfc}(z_{soa}, i; \tau, \tilde{\rho}_0, \tilde{\rho}_c, \tilde{k}, \tilde{\Theta}_{HG})}$$

Equation 55

where the index i designates the slot number, and $W_{inv}(i)$ is a weighting function equal to 1 by default. Since the angular function $\tilde{\rho}_{sfc}(z_{soa}, -\mu, \mu_0, \varphi - \varphi_0; \tau, \tilde{\rho}_0, \tilde{\rho}_c, \tilde{k}, \tilde{\Theta}_{HG})$ in Equation 52 is a function of $\tilde{\rho}_0$, an iteration procedure is applied to solve Equation **55** until the convergence criterion $\left|\rho_0^{itn} - \rho_0^{it(n+1)}\right| \leq 10^{-3}$ is satisfied. This convergence is in most of the cases achieved in three iterations or less.

3.6.3 Cost function definition

Finding the value of x that minimises the difference between the measurement vector $R_{Msat}(z_{sat}, i)$ and the forward model $R_M(z_{sat}, -\mu, \mu_0, \varphi - \varphi_0; U_{O3}, U_{H2O}, \tau, \tilde{\rho}_0, \tilde{k}, \tilde{\Theta}_{HG})$ is obtained for a χ^2 metrics that defines the cost function. Neglecting the angular notation, this function is written:

$$\chi^2 = \sum_i \left(\frac{RMsat\ (zsat, i) - RM(zsat, -\mu, \mu 0, \varphi - \varphi 0;\ UO3, UH2O, \tau, \tilde{\rho} 0, \tilde{k}, \tilde{\Theta} HG)}{\sigma_y(t)} \right)^2$$

Equation 56

where $\sigma_y(t)$ represents the measurement error. The number of degrees of freedom of χ^2 is defined as $v = Ny - Nx$ where N_x is the number of elements of the state vector ***x***. This number is four in the present retrieval system.

3.6.4 Measurement error: general definition

The measurement error σ_y includes both the instrumental uncertainty and the forward model approximations. The radiometric error has several different contributions. The first one is, of course, the radiometric noise of the instrument resulting from the dark current and other undesired electronics effects. The digitalisation level is also considered a source of error. It is equal to 64 levels (6 bits data) for Meteosat-2 observations and 256 levels (8 bits data) for Meteosat-7 observations. As daily observations are assumed to be virtual instantaneous measurements, it is necessary to translate image geo-location inaccuracies into equivalent radiometric error (see Section 3.6.4.3). Similarly, the actual aerosol load is subject to change during the daily accumulation of the measurement vector. Indeed, the longer this accumulation period, (which is the elapsed time between the first and the last clear-sky observation), the higher the probability that the aerosol load varies. Possible daily variations of the aerosol load are thus considered as measurement errors. An aerosol daily autocorrelation function is introduced to convert these changes into an equivalent radiometric error. Hence, the total measurement error $\sigma_y(t)$ of a pixel acquired at time t is dynamically estimated as the contributions of the following:

- the detector radiometric noise σ_I;
- the digitalisation error σ_D;
- the rectification uncertainty σ_R;

- the aerosol daily autocorrelation σ_A, and
- the forward model error σ_F.

Making the very strong assumption that these terms are not correlated, the total measurement error is expressed by:

$$\sigma_{\mathbf{y}}(t) = \sqrt{\sigma_{\mathbf{I}}^2(t) + \sigma_{\mathbf{D}}^2(t) + \sigma_{\mathbf{R}}^2(t) + \sigma_{\mathbf{A}}^2(t) + \sigma_{\mathbf{F}}^2(t)}. \quad \textit{Equation 57}$$

The terms $\sigma_{\mathbf{I}}$, $\sigma_{\mathbf{D}}$ and $\sigma_{\mathbf{R}}$ characterise the observation errors whereas the terms σ_A and σ_F represent the model assumption and forward modelling errors. The uncertainty on the model parameters (TCWV and TCO3) are not explicitly estimated but are included in the term σ_F. The dependence of the surface parameter characterisation on the actual position of the angular sampling is not included in the measurement error. A previous study has shown that errors that might result from an insufficient angular sampling remain small compared to σ_y (Lattanzio et al., 2006 [RD 15].

3.6.4.1 Detector Noise σ_I

During the processing of a row image conversion into a rectified image (referred to as level 1.5 data), an equalisation process takes place between the histogram of the two detectors. The process minimises any difference in the detector sensitivity. Hence, the radiometric error of the VIS band includes the contribution of the detector noise and their sensitivity difference, as shown in formula 6 below:

$$\sigma_{\mathbf{I}}(t) = \mathbf{y}_m(t)\,\frac{\sigma_{K_{1.5}}(t)}{K(t) - \overline{K}_0(t)} \quad \textit{Equation 58}$$

where:

K	is the digital count value
$\overline{K}_0$	is the mean space count value
$\sigma_{K1.5}$	the level 1.5 radiometric noise after the rectification and detector equalisation process

For MVIRI, the radiometric noise is written:

$$\sigma_{K_{1.5}}(t) = \mathbf{y}_m(t)\sqrt{\frac{1}{8}\sum_{c=1}^{8}\left(\sigma_{\overline{K}_0}(c)\right)^2 + \left(\frac{\overline{K}_{01}(t) - \overline{K}_{02}(t)}{2}\right)^2} \quad \textit{Equation 59}$$

where $\bar{\sigma}_{K_0}(c)$ is the mean space count standard deviation of one detector over one corner. K_{0_n} is the mean space value of detector n linearly averaged over the four space corners. The first term of the right hand side accounts for individual detector noise; the second term represents the difference between the detectors. There are only two detectors for the VIS band on the MVIRI instrument.

3.6.4.2 Digitalisation Noise σ_D

This term accounts for the digitalisation of the observed radiances in count values K on b bits. The corresponding digitalisation uncertainty is this:

$$\sigma_{\boldsymbol{D}}(t) = \boldsymbol{y}_m(t)\,\frac{0.5\,D_f}{K(t) - \overline{K}_0(t)} \qquad \textit{Equation 60}$$

where $D_f = 2^8/2^b$, 256 digitalisation levels (8 bits data) being taken as the reference.

3.6.4.3 Rectification Noise σ_R

As daily observations are assumed to be virtual instantaneous measurements, it is necessary to account for image rectification inaccuracies that can occur during the course of the day. For a pixel located at a position (p_1, p_2), these inaccuracies are converted into an equivalent radiometric noise:

$$\sigma_{\boldsymbol{R}}(t,p_1,p_2) = \boldsymbol{y}_m(t)\,\frac{1}{K(t,p_1,p_2) - \overline{K}_0(t)}\,\sqrt{\left(\frac{\partial K(t,p_1,p_2)}{\partial p_1}\sigma_{p_1}(t)\right)^2 + \left(\frac{\partial K(t,p_1,p_2)}{\partial p_2}\sigma_{p_2}(t)\right)^2} \qquad \textit{Equation 61}$$

where $\sigma_{p1}(t)$ and $\sigma_{p2}(t)$ are the root mean square error between landmarks identified in the rectified image and their actual earth location along the p_1 and p_2 direction respectively.

3.6.4.4 Equivalent Aerosol Optical Thickness (EAOT) Autocorrelation error σ_A

The longer the duration between the first and the last clear sky images, the higher the probability that the aerosol load actually varies. Analysis of Aerosol Robotic NETwork (AERONET) (Holben et al., 1998 [RD 12]) time series revealed that stable daily aerosol load typically corresponds to a temporal autocorrelation of 0.95 between two successive Meteosat observations. These changes introduce perturbations in the observed signal since the daily time series is assumed to have been instantaneously acquired. Such deviation from the algorithm assumptions can be converted into an equivalent radiometric error. Assuming that the daily aerosol load variations are represented by a first order autoregressive model, the AOT τ at slot $t + dt$ can be expressed as a function of AOT at slot t.

$$\tau(t+dt) = \alpha\tau(t) + \beta(t) = \tau(t) + (\alpha - 1)\tau(t) + \beta(t) \qquad \textit{Equation 62}$$

where:

α	is the autocorrelation
β	a random noise with a mean equal to zero

In the same way, we have:

$$\tau(t+2dt) = \alpha(\alpha\tau(t)+\beta(t))+\beta(t+2dt) \quad \text{Equation 63}$$

$$\tau(t+3dt) = \alpha(\alpha(\alpha\tau(t)+\beta(t))+\beta(t+2dt))+\beta(t+3dt) \quad \text{Equation 64}$$

$$\tau(t+h) = \alpha^h\tau(t)+\alpha^{h-1}\beta(t)\cdots+\beta(t+h) \quad \text{Equation 65}$$

Assuming that $\beta = 0$ and neglecting the changes in the illumination direction between two successive slots, the equivalent radiometric error at slot t + h is equal to:

$$y(\tau(t+h)) = y(\tau(t)+(\alpha-1)\tau(t)) \quad \text{Equation 66}$$

or, assuming a local linear behaviour of $y(\tau(t))$:

$$y(\tau(t)) = y(\tau(t))+\frac{\partial y(\tau(t))}{\partial\tau}((\alpha^h-1)\tau(t)) \quad \text{Equation 67}$$

The change $\partial y(\tau)/\partial\tau((\alpha^h-1)\tau(t))$ from slot t to $t + h$ is thus an undesired perturbation that can be considered as a radiometric noise of the measurement system. The corresponding relative auto correlation radiometric error for any slot $t_m = m + h$ is written as follows:

$$\sigma_{\boldsymbol{A}}(t) = \frac{\partial y(\tau(t))}{\partial\tau}\left((\alpha^h-1)\tau(t_m)\right) \quad \text{Equation 68}$$

where $t_m = (t_{min} + t_{max})/2$ with t_{min} the first slot and t_{max} the last slot not under-illuminated during the day. Large aerosol load variations are not covered by this method.

3.6.4.5 The forward model error σ_F

As seen in Section 2.1, the state variables k, Θ, τ have been discretized at intervals Δk, $\Delta\Theta$, $\Delta\tau$ to speed up the retrieval process. This discretisation is responsible for an error:

$$\sigma_{\boldsymbol{F}}(t) = y(t;\boldsymbol{x},\boldsymbol{b})\sqrt{\left(\frac{\partial y(t;\boldsymbol{x},\boldsymbol{b})}{\partial k}\frac{\Delta k}{2}\right)^2+\left(\frac{\partial y(t;\boldsymbol{x},\boldsymbol{b})}{\partial\Theta}\frac{\Delta\Theta}{2}\right)^2+\left(\frac{\partial y(t;\boldsymbol{x},\boldsymbol{b})}{\partial\tau}\frac{\Delta\tau}{2}\right)^2} \quad \text{Equation 69}$$

The discretisation steps Δk, $\Delta\Theta$, $\Delta\tau$ should be small enough so that this condition and the discretisation:

$$\sigma_F(t) \ll \sqrt{\sigma_{\boldsymbol{I}}^2(t) + \sigma_{\boldsymbol{D}}^2(t) + \sigma_{\boldsymbol{R}}^2(t)} \qquad \textit{Equation 70}$$

However, this condition is not always true as it is not possible to explore a very large number of solutions, limiting thereby the discretisation steps. It is thus necessary to account for the source of error σ_F. Equation 69 is estimated only once, to avoid being computed for each pixel and slot.

3.7 Description of the Data Interpretation Module (DIM)

3.7.1 Physics of the problem

This section describes the approach used to identify the acceptable solutions (one solution corresponds to a set of values for the parameters of the RPV model, $\tilde{\rho}_0$, $\tilde{k}$, $\tilde{\Theta}_{HG}$, and the associated optical depth value for the aerosol) to the inverse radiation transfer problem, and report the results in terms of the "likely" solution and statistics about the distribution of acceptable solutions.

When implementing the LUT approach to store the pre-computed values of the atmospheric functions intervening in Equation 52, the number and type of solutions are selected *a priori*. This implies that the accuracy of the solution depends on the discretisation of the LUTs, in particular with respect to the state variables which control the radiation transfer regime. In other words, the discretisation of the LUTs must be sufficiently fine to ensure at least one successful retrieval, but it must not be so fine as to limit the number of solutions which are radiatively equivalent–in the sense that they cannot be distinguished on the basis of the remote sensing data.

In general, more than one solution may be found to describe jointly the surface BRF field and the aerosol optical depth value. For example, it can be expected that the consideration of two slightly different atmospheric profiles will result in the identification of two classes of acceptable solutions for a given pixel. This ambiguity will increase with a finer discretisation of the LUTs, but also with a poorer spectral and angular sampling of the TOA radiance field. In addition, there are inherent limits to the determinability of some model parameters, independently from the approach followed for data interpretation. This is due to radiation transfer processes: two or more geophysical situations, represented by different sets of state variables, may very well lead to indistinguishable TOA BRF fields. Such situations often occur around the so-called "neutral points" for which any small variation in the aerosol optical depth value will not translate into significant changes in TOA BRF fields.

Past experience (see Kaufman and Sendra 1988 [RD 13], and King et al. 1992 [RD 14]) shows that the retrieved aerosol optical depth values will be more reliable over spectrally-dark surfaces than over the bright targets. The wide spectral response of the Meteosat sensor tends to dilute the spectral and directional signatures of the aerosol and is, therefore, not optimal for retrieving the aerosol optical depth values. The Surface Albedo algorithm will, in fact, retrieve the effective aerosol optical depth values – the values required to interpret the radiation fields in the coupled surface-atmosphere system using the forward modelling approach described in Section 3.6.2.

The DIM implemented in the Surface Albedo algorithm identifies all solutions acceptable to the retrieval process using the values of the χ^2 function (Equation 56) and selects the "likely" solution amongst this ensemble. After a screening of the χ^2 values, DIM will set a flag to indicate one of these cases: at least one of the χ^2 values is less than 1, or none of the χ^2 values are less than 1.

3.7.2 Mathematical implementation

The solution of the coupled surface-aerosol scattering problem is obtained dynamically during the retrieval based on the pre-computation of the function $\breve{\rho}_s(z_a, \Omega_s(t), \Omega_v; \tau, \boldsymbol{x}_s)$ for a set of pre-defined Θ, k and τ values listed in Table 4. For each of these pre-defined solutions $\boldsymbol{x}(j)$, the corresponding value of $\rho_0(j)$ is estimated first with Equation 55. The values of $\chi^2(\boldsymbol{x}(j))$ given by Equation 56 are calculated next for each of these solutions j. As the number of degrees of freedom of $\chi^2(\boldsymbol{x}(j))$ can vary from pixel to pixel, it is not possible to establish a unique minimum threshold value below which a value of $\chi^2(\boldsymbol{x}(j))$ constitutes an acceptable solution. Assuming a Gaussian distribution of the summation terms of the cost function Equation 56, the distribution of $\chi^2(\boldsymbol{x})$ can be represented by an incomplete Gamma function. The probability of finding an $\chi^2(\boldsymbol{x}(j))$ value smaller than a given threshold value χ_a^2 is expressed by:

$$P_a(\chi^2(\boldsymbol{x}(j)) < \chi_a^2, \nu) = 1 - \frac{1}{2^{\nu/2}\Gamma(\nu/2)} \int_0^{\chi_a^2} e^{-a/2} t^{\nu/2-1} da \qquad \textit{Equation 71}$$

where Γ is the Gamma function.

From this expression, it is possible to define the probability that the model parameters fit the observations by chance. A small probability should be interpreted as a poor agreement between the observations and the forward model. As the number of degrees of freedom decreases, the χ_a^2 value decreases, yielding a constant confidence in the solution.

Let us now define $\chi^2(P_a,\nu)$, the value of χ^2 corresponding to a probability P_a for ν degrees of freedom and $\mathcal{L}_a$ the ensemble of solutions $\{\boldsymbol{x}(l)\}$ satisfying the condition:

$$\mathcal{L}_a = \{\chi^2(\boldsymbol{x}(j)) < \chi^2(P_a, \nu)\}. \qquad \textit{Equation 72}$$

Only solutions with a probability higher than a defined threshold value P_a are considered as acceptable. In this ensemble of valid solutions $\mathcal{L}_a$, the most likely solution $\hat{x}$ is chosen as the one with the smallest χ^2 value, except if the dispersion of acceptable solutions is too large (Pinty et al, 2000a [RD 23]). In that case, the selection of the most likely solution is the one with the smallest χ^2 value whose ρ_0 value falls in the interval $\rho_0 \in \bar{\rho}_0 \pm \sigma_{\rho 0}$ where $\bar{\rho}_0$ is weighted mean value of the $\rho_0(l)$ values in $\mathcal{L}_a$ and $\sigma_{\rho 0}$ the weighted standard error estimated with the following:

$$\sigma_{\bar{\rho}_0} = t_{P_a/2}(L_a - 1) \sqrt{\sum_{l=1}^{L_a} \kappa_t(l)\,(\rho_0(l) - \bar{\rho}_0)^2} \qquad \textit{Equation 73}$$

where:

L_a	is the number of solutions in the ensemble $\mathcal{L}_a$
$t_{P_a/2}(L_a-1)$	is the Student coefficient for the 2-tails distribution with L_a-1 degrees of freedom

The weight κ_t is equal to:

$$\kappa_t(l) = \frac{\chi^2(P_a,\nu) - \chi^2(\boldsymbol{x}(l))}{\sum_{l=1}^{L_a}\left(\chi^2(P_a,\nu) - \chi^2(\boldsymbol{x}(l))\right)}. \qquad \textit{Equation 74}$$

The maximum probability P_a that defines the ensemble of acceptable solutions could not be selected arbitrarily but is constrained by the measurement uncertainty. This relationship is examined in Section 3.7.2.1.

3.7.2.1 Retrieval error estimation

The surface parameter error estimation allows the assessment of the DHR retrieval uncertainty and therefore supports a meaningful temporal analysis of surface albedo data sets derived from different instruments. In this analysis, systematic errors such as those resulting from calibration uncertainties are not taken into account in the retrieval process.

A statistical approach is proposed here for the estimation of the error $\sigma\hat{x}$ of the retrieved solution $\hat{x}$. Due to the measurement error σ_y, a solution $\hat{x}'$ close to the actual solution $\hat{x}$ could not necessarily be considered significantly different. Following similar reasoning found in Section 2.7, the error σ_y defines an ensemble of solutions $\mathcal{L}_{\sigma_y}$ that are not discriminable and are significantly different. This ensemble of solutions $\{\boldsymbol{x}(m)\}$ can be defined by the condition:

$$\mathcal{L}_{\sigma_y} = \{\chi^2(\boldsymbol{x}) < \chi^2(P_{\sigma_y},\nu)\}. \qquad \textit{Equation 75}$$

where $P\sigma_y$ is the corresponding probability, yet to be defined. Conceptually, the threshold value $\chi^2(P\sigma_y,\nu)$ should be equal to $\chi^2(\hat{x}+\sigma\hat{x})$. The average value of $\chi^2(\hat{x}+\sigma\hat{x})$ can be approximated by the formula that follows: (Govaerts and Lattanzio 2007 [RD 10]):

$$\langle\chi^2(\hat{\boldsymbol{x}}+\sigma_{\hat{\boldsymbol{x}}})\rangle \approx \frac{\langle y(\hat{\boldsymbol{x}}+\sigma_{\hat{\boldsymbol{x}}}) - \boldsymbol{y}_m\rangle}{\sigma_{\boldsymbol{y}}} = \chi^2(\hat{\boldsymbol{x}}) + \langle\chi^2(\hat{\boldsymbol{x}})\rangle \qquad \textit{Equation 76}$$

Where $\langle\chi^2(\hat{x})\rangle$ is the average value of $\chi^2(\hat{x})$ over many processed pixels (~10^6).

The ensemble of solutions $\boldsymbol{x}(m) \in \mathcal{L}\sigma_y$ that are not discernable with respect to the measurement error σ_y is thus defined by the condition:

$$\mathcal{L}_{\sigma_y} = \{\chi^2(\boldsymbol{x}(m)) \le \chi^2(\hat{\boldsymbol{x}}) + t_{P_{\alpha/2}}(\infty)\,\langle\chi^2(\hat{\boldsymbol{x}})\rangle\}. \qquad \textit{Equation 77}$$

Let us now examine the relationship between P_a and $P_{\sigma y}$. All elements in the ensemble $\mathcal{L}_{\sigma y}$ should constitute acceptable solutions which translates into the condition $\mathcal{L}_{\sigma y} \subseteq \mathcal{L}_a$. The probability P_a has thus to be chosen to satisfy the inequality:

$$\chi^2(P_{\sigma_y}, \nu) = \chi^2(\hat{\boldsymbol{x}}) + t_{P_a}(\infty)\ \langle \chi^2(\hat{\boldsymbol{x}}) \rangle \ \leq\ \chi^2(P_a, \nu). \qquad \textit{Equation 78}$$

$P_{\sigma y}$ constitutes the maximum acceptable probability which, in turn, determines the minimum acceptable $\chi^2(P_{\sigma y},\nu)$ value as a function of the measurement error σ_y. To increase the spatial coverage of the generated products, this probability is decreased when no solution satisfies Equation 77, when $\mathcal{L}_{\sigma y}$ is empty. Pixels processed with this decreased probability should be considered as backup solutions and carefully interpreted. Hence, $P_{\sigma y}$ is used as a quality indicator of the solution reliability, accounting for both the measurement error and the actual number of available observations.

The error $\sigma\hat{x}$ is defined by the distribution of the ensemble of solutions $x(m) \in \mathcal{L}_{\sigma y}$ with this:

$$\sigma^2_{\hat{\boldsymbol{x}}} = t_{P_a}(L_{\sigma \mathbf{y}} - 1)\sigma^2_{\boldsymbol{x}} + \left(\frac{\partial y(t;\hat{\boldsymbol{x}},\boldsymbol{b})}{\partial \hat{\boldsymbol{x}}}\frac{\Delta \hat{\boldsymbol{x}}}{2}\right)^2 \qquad \textit{Equation 79}$$

where:

$L_{\sigma y}$	is the number of solutions in $\mathcal{L}_{\sigma y}$
σ^2_x	σ^2_x is the standard deviation of $\boldsymbol{x}(m)$

The second term of the right hand side part of Equation 79 represents the error due to the discretisation of the $\boldsymbol{x}$ space. This term is equal to zero for the ρ_0 parameter.

3.8 Description of the Space-time Averaging Module (SAM)

3.8.1 Physics of the Problem

This section describes the technique applied to generate temporal compositing quantities from the daily products at full resolution. The objective of the temporal compositing is to maximise the number of clear sky processed pixels during a 10-day period. This compositing relies on the selection of the most representative solution over the accumulation period.

3.8.2 Mathematical implementation

One way is to select the solution with the best fit accounting for the actual number of degrees of freedom. Hence, the most representative solution $\hat{x}$ within a 10-day period is the one with the highest probability. However, as clouds tend to increase the signal received at the satellite level, selecting the solution with the smallest $\hat{\rho}_0$ will tend to minimise the impact of undetected clouds. Thus, if two or more solutions have the same probability, the one with the lowest $\overline{\hat{\rho}_0}$ is selected.

Surface albedo is generally not expected to undergo important changes during a 10-day period so that the repetition of the same measurement might be assumed from day to day. Under these conditions, the temporal stability of the solution during a compositing period should increase the user confidence in the retrieved product. The error of the most representative solution $\hat{x}$ is as follows:

$$\sigma_{\overline{\hat{\boldsymbol{x}}}} = \frac{t_{P_a/2}(N_T - 1)}{\sqrt{N_T}} \sqrt{\sum_{d=1}^{N_T} \hat{\kappa}_T(d)(\hat{\boldsymbol{x}}(d) - \overline{\hat{\boldsymbol{x}}})^2} \qquad \textit{Equation 80}$$

Where N_T is the number of days with an acceptable solution during the compositing period. The normalised weight $\hat{\kappa}_T(d)$ is estimated as follows:

$$\hat{\kappa}_T(d) = \frac{1}{P(\hat{\boldsymbol{x}}(d))} \qquad \textit{Equation 81}$$

Where $P(\hat{\boldsymbol{x}}(\mathrm{d}))$ is the probability of the solution $\hat{\boldsymbol{x}}$ of day d. It is thus expected that the uncertainty of the retrieved solution decreases as the number of days increases except for those places that are subject to drastic temporal changes in surface albedo as is in case of wildfires (Govaerts, 1999 [RD 7]) When only one likely solution has been found during the compositing period, $\overline{\sigma\hat{\boldsymbol{x}}}$ is set equal to $\sigma\hat{\boldsymbol{x}}$.

3.8.2.1 Surface Albedo Estimation

The Directional Hemispherical Reflectance can be written as follows:

$$\mathrm{DHR}(\theta_0 = 30°) = \int_{2\pi} \rho_s(z_0, \Omega_s, \Omega'; \overline{\hat{\boldsymbol{x}}}_s) d\Omega' = \overline{\hat{\rho}_0} \int_{2\pi} \breve{\rho}_s(z_0, \Omega_s, \Omega'; \overline{\hat{k}}, \overline{\hat{\Theta}}) d\Omega' \qquad \textit{Equation 82}$$

and is calculated for a sun position fixed at 30°. Assuming that the errors on $\hat{\boldsymbol{x}}_s$ are not correlated, the non-systematic error on the estimation of the DHR is expressed with the following:

$$\sigma_{\mathrm{DHR}} \approx \sqrt{\left(\frac{\partial \mathrm{DHR}}{\partial \rho_0} \sigma_{\overline{\hat{\rho}_0}}\right)^2 + \left(\frac{\partial \mathrm{DHR}}{\partial \Theta} \sigma_{\overline{\hat{\Theta}}}\right)^2 + \left(\frac{\partial \mathrm{DHR}}{\partial k} \sigma_{\overline{\hat{k}}}\right)^2}. \qquad \textit{Equation 83}$$

Since the variable of integration (the solid angle) is not derived, the derivation and integration operators can be exchanged, and Equation 84 is produced:

$$\sigma_{\mathrm{DHR}} = \left[\left(\int_{2\pi} \breve{\rho}_s(z_0, \Omega_s, \Omega'; \overline{\widehat{k}}, \overline{\widehat{\Theta}}) d\Omega' \, \sigma_{\overline{\widehat{\rho}_0}} \right)^2 + \left(\int_{2\pi} \frac{\partial \rho_s(z_0, \Omega_s, \Omega'; \overline{\widehat{x}}_s)}{\partial \Theta} \mathrm{d}\Omega' \, \sigma_{\overline{\widehat{\Theta}}} \right)^2 + \left(\int_{2\pi} \frac{\partial \rho_s(z_0, \Omega_s, \Omega'; \overline{\widehat{x}}_s)}{\partial k} \mathrm{d}\Omega' \, \sigma_{\overline{\widehat{k}}} \right)^2 \right]^{1/2}.$$

Equation 84

Additional information on this error estimation is in Govaerts and Lattanzio (2007) [RD 10].

3.8.2.2 Conversion to broadband albedo

This relationship between the derived Meteosat VIS band $\mathrm{DHR}_{\mathrm{VIS}}$ in shortwave (from 0.3 to 3.0 µm) broadband albedo $\mathrm{DHR}_{\mathrm{BB}}$ is given by a third order polynomial written:

$$\mathrm{DHR}_{\mathrm{BB}} = a + b\,\mathrm{DHR}_{\mathrm{VIS}} + c\,(\mathrm{DHR}_{\mathrm{VIS}})^2 + d\,(\mathrm{DHR}_{\mathrm{VIS}})^3$$

Equation 85

The empirical coefficients *a, b, c, d* for the DHR conversion take the following values according to the Meteosat number (Loew and Govaerts, 2010 [RD 17]):

Met	*a*	*b*	*c*	*d*
2	-2.95364443e-05	1.22636437e+00	-1.45464587e+00	1.27798259e+00
3	-2.95364443e-05	1.32036722e+00	-1.52968502e+00	1.25365901e+00
4	-2.95364589e-05	1.22655797e+00	-1.07426369e+00	8.96015048e-01
5	-2.95364443e-05	1.25341415e+00	-1.09384084e+00	8.89843404e-01
6	-2.95364443e-05	1.30573940e+00	-1.31526375e+00	1.05711114e+00
7	-2.95364589e-05	1.26273489e+00	-1.11476350e+00	9.00940299e-01

Table 5: Empirical coefficients a–d for the DHR conversion

For the conversion of the $\mathrm{BHR}_{\mathrm{iso}}$, the empirical coefficients are as follows:

Met	*a*	*b*	*c*	*d*
2	-2.85976712e-05	9.81895685e-01	-8.48408699e-01	7.43798614e-01
3	-2.85976712e-05	1.09896255e+00	-1.07471538e+00	9.11732554e-01
4	-2.85976712e-05	1.00361478e+00	-6.55005634e-01	6.47315860e-01
5	-2.85976712e-05	1.04928327e+00	-7.66418219e-01	7.47902989e-01
6	-2.85976712e-05	1.15992260e+00	-1.13301563e+00	9.98916626e-01
7	-2.85976712e-05	1.03751910e+00	-6.88233614e-01	7.00615168e-01

Table 6: Empirical coefficients a–d for the BHR conversion

3.9 BHR_{iso} error estimation

The σBHR• error is currently not stored in the distributed product. This error can be calculated with the following expression:

$$\sigma_{\mathrm{BHR}_\bullet} \approx \sqrt{\sigma^2_{\hat{\rho}_0} + \left(\frac{\partial \alpha_0(\overline{\hat{k}}, \overline{\hat{\Theta}})}{\partial k}\,\sigma_{\overline{\hat{k}}}\right)^2 + \left(\frac{\partial \alpha_0(\overline{\hat{k}}, \overline{\hat{\Theta}})}{\partial \Theta}\,\sigma_{\overline{\hat{\Theta}}}\right)^2}$$

Equation 86

Where α_0 is tabulated with the following value:

h	Θ	k	α_0	h	Θ	k	α_0	h	Θ	k	α_0
0.15	–0.30	0.40	3.29568	0.15	–0.20	0.40	3.01252	0.15	–0.10	0.40	2.74655
0.15	–0.30	0.50	2.91138	0.15	–0.20	0.50	2.64497	0.15	–0.10	0.50	2.39410
0.15	–0.30	0.60	2.62286	0.15	–0.20	0.60	2.36857	0.15	–0.10	0.60	2.12919
0.15	–0.30	0.70	2.40092	0.15	–0.20	0.70	2.15551	0.15	–0.10	0.70	1.92501
0.15	–0.30	0.80	2.22700	0.15	–0.20	0.80	1.98812	0.15	–0.10	0.80	1.76452
0.15	–0.30	0.90	2.08885	0.15	–0.20	0.90	1.85469	0.15	–0.10	0.90	1.63641
0.15	–0.30	1.00	1.97802	0.15	–0.20	1.00	1.74715	0.15	–0.10	1.00	1.53294
0.15	–0.25	0.40	3.15165	0.15	–0.15	0.40	2.87767	0.15	–0.05	0.40	2.61871
0.15	–0.25	0.50	2.77600	0.15	–0.15	0.50	2.51782	0.15	–0.05	0.50	2.27346
0.15	–0.25	0.60	2.49365	0.15	–0.15	0.60	2.24720	0.15	–0.05	0.60	2.01425
0.15	–0.25	0.70	2.27618	0.15	–0.15	0.70	2.03856	0.15	–0.05	0.70	1.81463
0.15	–0.25	0.80	2.10550	0.15	–0.15	0.80	1.87455	0.15	–0.05	0.80	1.65780
0.15	–0.25	0.90	1.96964	0.15	–0.15	0.90	1.74369	0.15	–0.05	0.90	1.53264
0.15	–0.25	1.00	1.86037	0.15	–0.15	1.00	1.63808	0.15	–0.05	1.00	1.43151

and:

h	Θ	k	α0
0.15	0.00	0.40	2.49373
0.15	0.00	0.50	2.15556
0.15	0.00	0.60	1.90210
0.15	0.00	0.70	1.70718
0.15	0.00	0.80	1.55420
0.15	0.00	0.90	1.43218
0.15	0.00	1.00	1.33363

4 BRF AND BRF UNCERTAINTY: SPECTRAL AND BROADBAND

4.1 Spectral BRF

The MSA product contains also the RPV model parameters (K, THETA in Table 10) used to estimate the best solution and corresponding DHR (DHR30 in Table 9) value stored in the product. The RPV model is described in Section 3.6.2. The model definition is repeated here for clarity.

$$\rho_{sfc}(z_0, \Omega_0 \rightarrow \Omega; \rho_0, \rho_c, \Theta, k) = \rho_0 \, \check{\rho}_{sfc}(z_0, \Omega_0 \rightarrow \Omega; \rho_c, \Theta, k) \qquad \textit{Equation 87}$$

Where:

ρ_0 and $\check{\rho}_{sfc}(z_0, \Omega_0 \rightarrow \Omega; \rho_c, \Theta, k)$	describes the amplitude and the angular field of the surface BRF

This latter quantity is expressed by:

$$\check{\rho}_{sfc}(z_0, \Omega_0 \rightarrow \Omega; \rho_c, \Theta, k) = M_I(\theta_0, \theta; k)\, F_{HG}(g; \Theta_{HG})\, H(\rho_c; G) \qquad \textit{Equation 88}$$

Each parameter only appears in one single factor as defined in the following three equations:

$$M_I(\theta_0, \theta; k) = \frac{\cos^{k-1}\theta_0 \cos^{k-1}\theta}{(\cos\theta_0 + \cos\theta)^{1-k}} \qquad \textit{Equation 89}$$

$$F_{HG}(g; \Theta_{HG}) = \frac{1 - \Theta_{HG}^2}{[1 + 2\Theta_{HG}\cos g + \Theta_{HG}^2]^{3/2}} \qquad \textit{Equation 90}$$

$$H(\rho_c; G) = 1 + \frac{1 - \rho_c}{1 + G} \qquad \textit{Equation 91}$$

Where G is defined in Equation 6, θ_0 is the Sun Zenith Angle and θ is the View Zenith Angle.

The MSA product also contains the RPV model parameter uncertainties (ERR_K, ERR_T in Table 10) used to estimate the DHR uncertainty (Section 3.8.2.1).

The BRF depends on the measuring geometry, i.e. on the View and Sun Angle (see Figure 6). The View angle depends on the location on the pixel on Earth and on the position of the satellite (Sub Satellite Point).

If we consider that the RPV model parameters are retrieved following an accumulation during a full day to account for the intrinsic surface anisotropy, it is clear that several Sun positions (depending on the time the input satellite measurement has been acquired) are ingested. A user could then calculate

the BRF value for each time of the day (= Sun position) just applying the RPV BRF model using the retrieved model parameters and changing the Sun Angle.

In this section we consider a BRF value provided as a daily one, so a unique Sun Angle must be considered. The convention used in the MSA for the estimation of the DHR is to fix the Sun at 30°. See Section 3.8.2.1. Another convention is to use the Sun Angle at the local (pixel) noon. The latter is suitable if considering high latitude especially in winter when the Sun at 30° is not a typical situation. It is anyway important to stress that this is just a convention and not a rule. The daily BRF is calculated at the local noon. It is assumed that the surface does not change during the 10 days (compositing period for the MSA product) and the same RPV model parameters are used to calculate the daily BRF. The only parameter changing is the sun position at local noon.

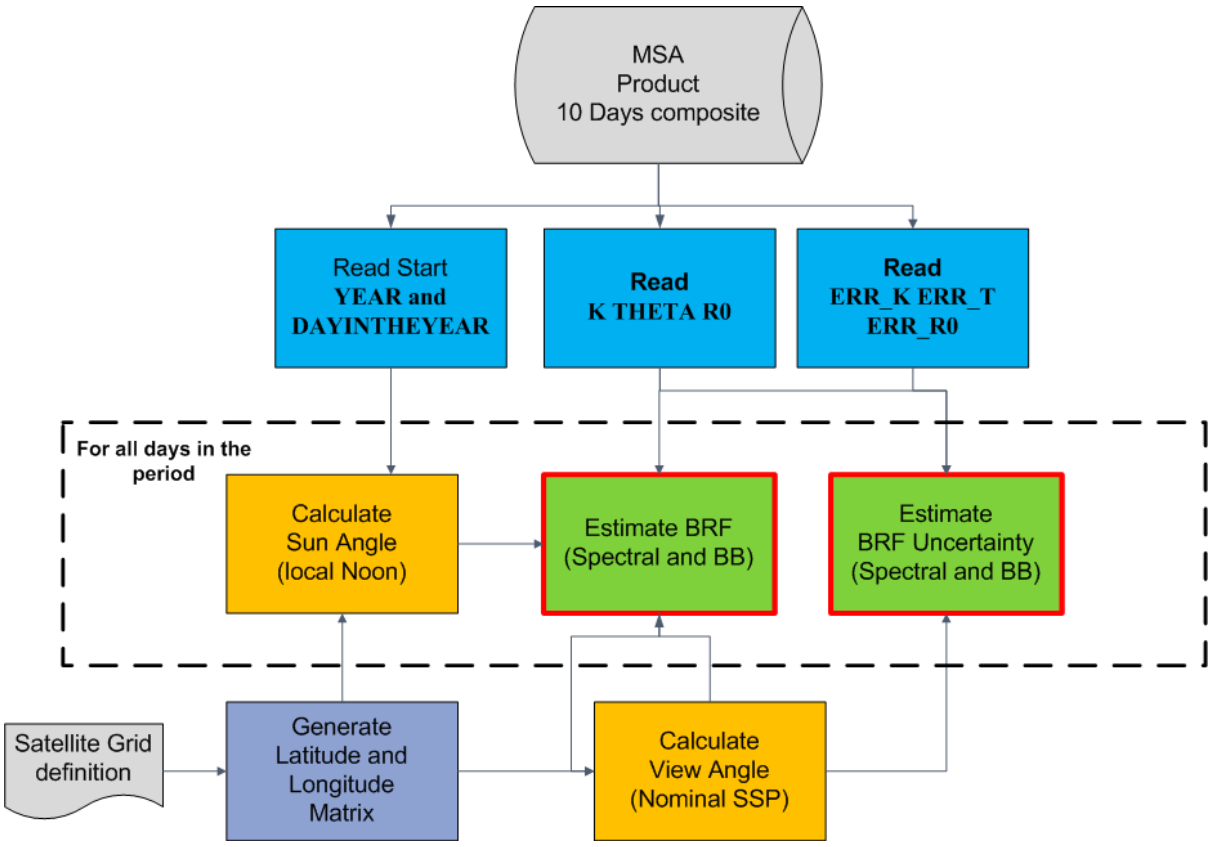

Figure 8: Conceptual steps to estimate the BRF and corresponding uncertainty. The Parameters BESTDAY, K, THETA, R0, ERR_K, ERR_T and ERR_R0 are defined in Table 10.

4.2 Spectral BRF Uncertainty

The RPV model is a semi-empirical representation of how a generic surface can reflect sun light. It is an analytical function and as such can be differentiated. The formula for the uncertainty is:

$$\sigma_{BRF} = \sqrt{(\frac{\delta BRF}{\delta \varrho_0}\sigma_{\varrho_0})^2 + (\frac{\delta BRF}{\delta \Theta_{HG}}\sigma_{\Theta_{HG}})^2 + (\frac{\delta BRF}{\delta k}\sigma_k)^2} \qquad \textit{Equation 92}$$

Where:

$$\frac{\delta BRF}{\delta \varrho_0} = M(k)F_{MG}(\Theta_{HG})H(\varrho_0)$$
$$\frac{\delta BRF}{\delta \Theta_{HG}} = \varrho_0 M(k)H(\varrho_0)\frac{\delta F_{MG}(\Theta_{HG})}{\delta \Theta_{HG}}$$
$$\frac{\delta BRF}{\delta k} = \varrho_0 F_{MG}(\Theta_{HG})H(\varrho_0)\frac{\delta M(k)}{\delta k}$$

Equation 93

The single functions derivatives are as follows:

$$\frac{\delta M(k)}{\delta k} = (cos\theta_0)^{k-1}(cos\theta)^{k-1}(cos\theta_0 + cos\theta)^{k-1}(log(cos\theta_0 + cos\theta) + \log(cos\theta_0) + \log(cos\theta))$$
$$\frac{\delta F_{MG}(\Theta_{HG})}{\delta \Theta_{HG}} = \frac{\Theta_{HG}(\Theta_{HG} - 5) - (\Theta_{HG} - 3)cosg}{(2\Theta_{HG}cosg + {\Theta_{HG}}^2 + 1)^{5/2}}$$

Equation 94

And $cosg$ is a function of the Satellite and Sun position:

$$cosg = cos\theta cos\theta_0 + sin\theta sin\theta_0 cos\varphi$$

Equation 95

Where φ represents the absolute value of the difference between the Sun and Satellite position azimuth angle.

4.3 Broadband BRF and BRF uncertainty

The MSA retrieval is performed on the native VIS Meteosat spectral band. See Figure 1. As described for the DHR in Section 3.8.2.2, also for the BRF a conversion to shortwave (from 0.3 µm to 3.0 µm) broadband should be applied to obtain a value that can be compared with similar retrieval performed with other instruments.

The relation between Spectral BRF and DHR repeated here for clarity is given in Section 3.6.1 :

$$DHR(z_0, \mu_0) = \frac{1}{\pi}\int_{\Omega} \rho_{sfc}(z_0, \Omega' \rightarrow \Omega)\mu' d\,\Omega'$$

Equation 96

The Conversion to Broadband is obtained using a polynomial relation of degree 3:

$$DHR_{BB} = P^3(DHR_{VIS}) = a_0 + a_1(DHR_{VIS}) + a_2(DHR_{VIS})^2 + a_3(DHR_{VIS})^3$$

Equation 97

This approach is described in Loew and Govaerts (2010) [RD 17].

A similar approach can be applied to the BRF conversion to Broadband using the same polynomial relation used in Equation 96:

$$BFR_{BB} = P^3(BRF_{VIS}) = a_0 + a_1(BRF_{VIS}) + a_2(BRF_{VIS})^2 + a_3(BRF_{VIS})^3$$ *Equation 98*

Due to the non-linear behavior of the Spectral to Broadband conversion in the case of MVIRI, the application of such relation introduces a systematic error.

$$DHR_{BB}^{BRF} = \frac{1}{\pi}\int_{\Omega} P^3(\rho_{sfc}(z_0, \Omega' \rightarrow \Omega))\mu' d\,\Omega' \neq DHR_{BB}$$
$$= P^3(\frac{1}{\pi}\int_{\Omega} \rho_{sfc}(z_0, \Omega' \rightarrow \Omega)\mu' d\,\Omega')$$ *Equation 99*

At the present it has been decided to use for the shortwave broadband conversion of the BRF the same method and coefficients used for the DHR conversion. An estimate of the uncertainty due to this approach is included in the total uncertainty estimation for this parameter. For this purpose the variable defined in Equation 97 has been estimated for all the possible values of the RPV model parameters (ρ_0, K, Θ_{HG}) used in the MSA retrieval scheme and for some values of the Sun Zenith angle (SZA). The total number of cases is 2401 (7 × 7 × 7 × 7).

ρ_0	0.05, 0.1, 0.150, 0.2, 0.25, 0.3
K	0.4, 0.5, 0.6, 0.7, 0.8, 0.9, 1.0
Θ_{HG}	–0.30, –0.25, –0.20, –0.15, –0.10, –0.05, 0.00
SZA	10., 20., 30., 40., 50., 60., 70.

Table 7: Parameters values used for the estimation of the Broadband conversion uncertainty. The total number of cases is 2401.

The same values of the parameters have been used to estimate the Broadband DHR from a Broadband BRF:

$$DHR_{BB}^{BRF} = \frac{1}{\pi}\int_{\Omega} P^3(\rho_{sfc}(z_0, \Omega' \rightarrow \Omega))\mu' d\,\Omega'$$ *Equation 100*

In performing this calculation all BRF values higher than 1 have been cut (BRF correction). Such high BRF values can occur in very special conditions without breaking any physical law.

The absolute relative percentage difference ($\sigma_{BB}(\rho_{0,SZA})$) between Equation 97 and Equation 100 as a function of the reflectance level ρ0 and the Sun Zenith Angle (SZA) is assumed to be an estimation of the uncertainty due to the application of such a method for the conversion to shortwave broadband. This quantity has been obtained averaging the values for all K and Θ_{HG} for each couple $\rho_{0,SZA}$. The absolute percentage uncertainty is shown in Figure 9. Similar relations have been found for all other Meteosat First Generation satellites.

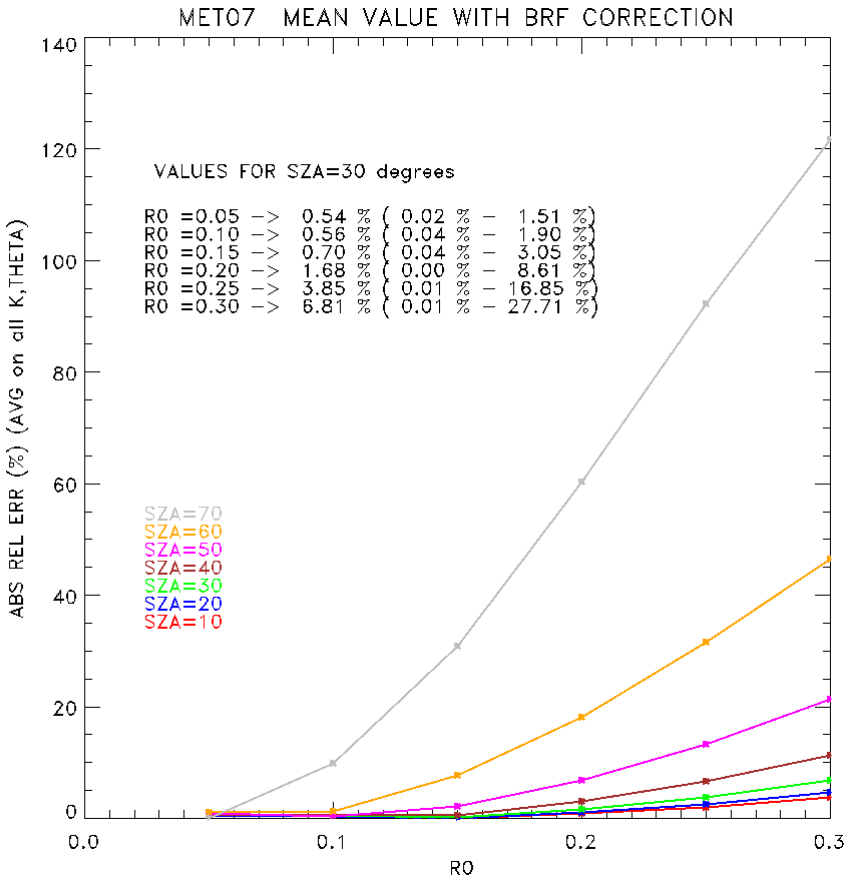

Figure 9: Absolute relative percentage error as a function of the Sun Zenith Angle and the RPV Reflectance level for MET07. A threshold to the BRF (if BRF >1 then BRF=1) before conversion to Broadband has been applied to limit the uncertainty for very high (> 0.6) albedo values.

The total uncertainty on the shortwave Broadband BRF σ_{BRF}^{BB} is given by two factors:

$$\sigma_{BRF}^{BB} = \sqrt{(\frac{\delta BRF_{BB}}{\delta BRF_{VIS}} \sigma_{BRF_{VIS}})^2 + (\sigma_{BB}\,(\rho_0, \mathrm{SZA}))^2}$$

where:

$$\frac{\delta BRF_{BB}}{\delta BRF_{VIS}} = a_1 + 2a_2(BRF_{VIS}) + 3a_3(BRF_{VIS})^2$$

and

$$\sigma_{BB}\,(\rho_0, \mathrm{SZA}) = \langle 100. \frac{\left| DHR_{BB}^{BRF}(K, \Theta_{HG}) - DHR_{BB}(K, \Theta_{HG}) \right|}{DHR_{BB}(K, \Theta_{HG})} \rangle$$

Equation 101

4.4 Spectral and Broadband BRF: SEVIRI

The Spinning Enhanced Visible and InfraRed Imager (SEVIRI) on board Meteosat Second Generation is a 12-channel imager (Schmetz et al., 2002, [RD 30]).

Following the method described in Govaerts et al., 2006 [RD 9] the shortwave broadband albedo can be derived as a linear combination of the two SEVIRI Visible channels, VIS06 and VIS08.

$$DHR_{BB} = L(DHR_{VIS06}, DHR_{VIS08}) = a_0 + a_1 DHR_{VIS06} + a_2 DHR_{VIS08} \quad \textit{Equation 102}$$

The relation is shown in Figure 10.

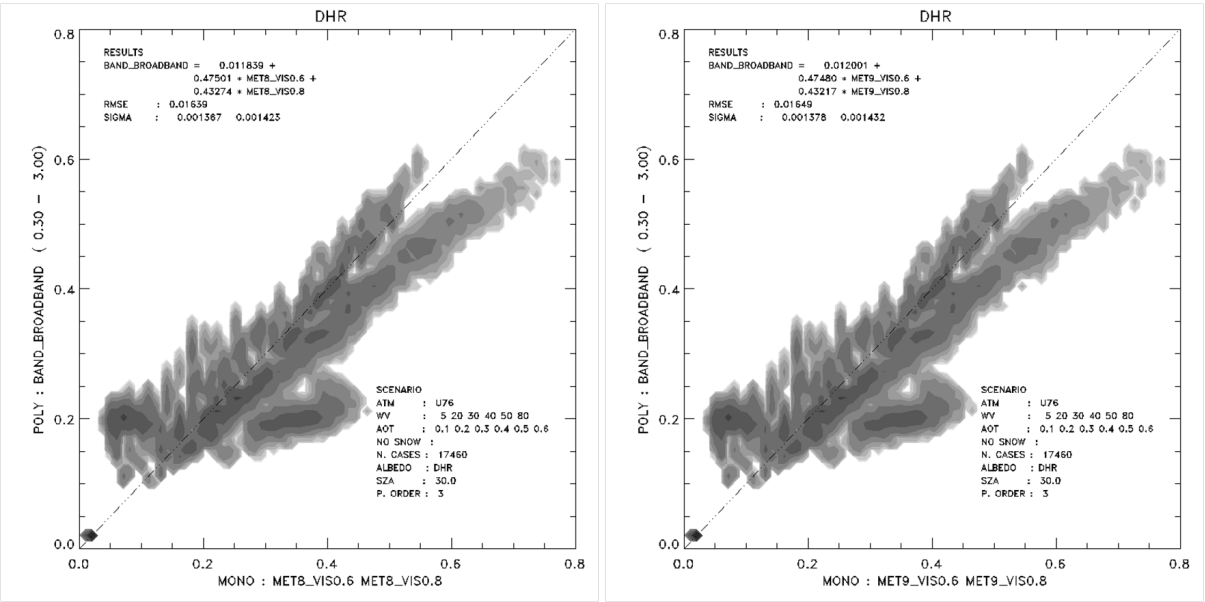

Figure 10: Relation between the VIS06 and VIS08 SEVIRI channels and the shortwave broadband DHR value for Meteosat 8 (left panel) and Meteosat 9 (right panel).

The coefficient for the conversion to shortwave broadband are:

Met	*a0*	*a1*	*a2*
8	0.010178	0.47150	0.45715
9	0.012001	0.47480	0.43217

Table 8: Empirical coefficients to convert the DHR/BRF of SEVIRI Meteosat 8 and 9 from VIS06,VIS08 to shortwave broadband.

The Broadband DHR calculated as the integral of a linear combination of RPV BRF (for the VIS06 and VIS08 channels) is expressed in the following equation:

$$DHR_{BB}^{BRF} = \int_{\Omega} L(BRF_{VIS06}, BRF_{VIS08})\, d\Omega \quad \textit{Equation 103}$$

And $DHR_{BB} \equiv DHR_{BB}^{BRF}$ is true if:

$$BRF_{BB} = \frac{a_0}{\int_\Omega d\Omega} + a_1 BRF_{VIS06} + a_2 BRF_{VIS08}$$

Equation 104

The uncertainty on DHR_{BB}^{BRF} can be analytically calculated as follows:

$$\sigma_{BRF}^{BB} = \sqrt{\left(\frac{\delta BRF_{BB}}{\delta BRF_{VIS06}} \sigma_{BRF_{VIS06}}\right)^2 + \left(\frac{\delta BRF_{BB}}{\delta BRF_{VIS08}} \sigma_{BRF_{VIS08}}\right)^2}$$
$$= \sqrt{(a_1 \sigma_{BRF_{VIS06}})^2 + (a_2 \sigma_{BRF_{VIS08}})^2}$$

Equation 105

5 ASSUMPTIONS AND LIMITATIONS

5.1 Assumptions

The Surface Albedo algorithm described in this ATBD is based on the following assumptions:

- A one-dimensional horizontally homogeneous radiation transfer model is assumed adequate to represent the radiation transfer regime at the scale of a Meteosat pixel;
- The effects of topography and slope on the scattering functions are ignored;
- A "standard" type of atmosphere is considered accurate and generic enough to cover a variety of geophysical situations that may be encountered over the geographical area of interest. The default option is the US-62 atmosphere;
- The decoupling between gaseous absorption and aerosol scattering effects does not significantly affect the results;
- The atmospheric and surface properties do not vary significantly during the 24-hour daylight period;
- The RPV model is considered adequate to accurately represent all types of surface bidirectional reflectance factors at the scale of the Meteosat measurements;
- The MRPV model is assumed to be capable of representing any non-cloudy TOA BRF fields that will be sampled by the Meteosat instrument, with sufficient accuracy.
- The same RPV model parameters retrieved for an MSA compositing period (10 days) are used to estimate the daily BRF. It is assumed that the surface properties do not change drastically during the 10 days.

5.2 Limitations

The following limitations apply to the Surface Albedo algorithm proposed in this ATBD:

- The retrievals will be made only on the basis of data acquired when the illumination and observation zenith angles are less than 70 °;
- The cloud detection method described in Pinty et al., 2000b [RD 24] is based on the temporal analysis of the ToA BRF, and does not perform optimally when the cloud cover remains stable during an entire day. Consequently, some surface albedo pixels might still be contaminated by undetected clouds;
- Any significant variations, in the contents and properties of the atmospheric components controlling the radiation transfer processes over the Meteosat spectral response, which might occur during the daylight period, will decrease the quality and reliability of the results;
- All the surface retrieved quantities are weighted by the Meteosat spectral response;
- The accuracy and reliability of the results may vary with the digitization levels of the Meteosat instruments (6 or 8 bits);
- The accuracy of the results may vary with the spectral response of the various Meteosat instruments;
- The reciprocity principle is valid over terrestrial surfaces at a spatial resolution of a few kilometres.

- The current method for the estimation of the MVIRI Broadband BRF is affected by a systematic error due to the non linearity of the conversion formula. This error is kept into account in the estimation of the Broadband BRF uncertainty.

APPENDIX A SURFACE ALBEDO PRODUCT LIST

The MSA algorithm retrieves for each processed pixel 23 parameters. They are divided in two classes: Scientific dataset and Ancillary dataset. Members of the first group are the relevant scientific information, while the second contains additional information useful for quality check.

A.1 Scientific dataset

Name	*Description*
BHRiso	The isotropic Bi-Hemispherical Reflectance field contains the surface albedo in the Meteosat VIS band that would have been observed under isotropic illumination conditions for the best solution of day d with $\hat{\boldsymbol{x}}(d) = \hat{\boldsymbol{x}}$ of the compositing period.
DHR30	The Directional Hemispherical Reflectances field (`DHR30`) contains the surface albedo value for the best solution of day d with $\hat{\boldsymbol{x}}(d) = \bar{\hat{\boldsymbol{x}}}$ of the compositing period. It represents the *spectral albedo* in the Meteosat sensor VIS band spectral interval assuming a sun zenith angle of $\mu_0 = 30°$. Since the angle μ_0 is the same for all pixels throughout the year, the DHR is appropriate for the monitoring of the spatial or temporal changes of the surface radiative properties.
DHR30 error 10D	This field represents the estimated DHR error using the information on all available retrieval during a 10-day period.
Probability	This field contains the probability of the solution $\hat{\boldsymbol{x}}$ of the selected day d of the compositing period. Pixels with a probability smaller than 80 % or 90 % should not be considered when the MSA product is analysed.

Table 9: Scientific output dataset

A.2 Surface Albedo Ancillary Dataset

Name	*Description*
QUALITYFLAG	This flag takes the following values: ***Val*** ***Meaning*** 0 OK 1 No valid days in the period 2 No valid samples in the period 3 No likely day 4 Ivalid solution index 5 Dubious solution , $P_a(\hat{\boldsymbol{x}}(d)) = 0.1$ 6 Weak solution, $0.1 < P_a(\hat{\boldsymbol{x}}(\mathrm{d})) \leq 0$.
NUMSOL	The number of acceptable solutions. The value 255 is set for invalid pixels.
NSLOT	Number of inputs lots before cloud screening.
NSLOTASM	Number of clear sky input slots.
K	Parameter describing the shape of the surface BRF in the RPV model for the best fit.
THETA	Parameter describing the asymmetry of the surface BRF in the RPV model for the best fit.
AER_OPT_THICK	Estimated equivalent aerosol optical thickness.
R0	Amplitude of the surface BRF in the RPV model for best fit.
ERR_R0	Estimated error of $\overline{\hat{\rho}_0}$.
NUMDAYS	Actual number of days available in this period.
BESTDAY	Selected day during the compositing period.
Chi2DCP	Cost function of the cloud screening.
Chi2ASM	Cost function of the inversion.
DHRError	Estimated error of the DHR for the best day d.
ERR_K	Estimated error of parameter K
ERR_T	Estimated error of parameter THETA
ERR_OPT	Estimated error of parameter AER_OPT_THICK
AVGOPT	Average value of $\hat{\tau}$ during the compositing period.
ERR_AVG_ERR	Standard deviation of `AVGOPT`.
RADIOMETRIC NOISE	Mean daily radiometric noise of the best day *d* calculated with $(\Sigma_{Ny}\, \sigma_y(t))/N_y$

Table 10: Ancillary output dataset

APPENDIX B DESCRIPTION OF THE CRAF DATABASE

The pre-Computed RAdiative transfer Functions (CRAF) database stores the functions and parameters required by the ASM to perform the simulations of Meteosat-like observations. The CRAF database contains the various tables of numerical values used to compute Equation **52**. The identification and contents of each table is summarized in Table 11.

LUT	*Comment*	*Entry Point*	*Equation*	*Source*
BSRF	Intrinsic atmospheric reflectance factor	θ_S, θ_V, $\Delta\varphi$, τ	Equation 55: $\tilde{\rho}(z_{soa}, i; \tau)$	6S
DATF	Direct attenuation transmission factor for Sun (View) angle for direct radiation	θ_S, (θ_V), τ	Equation 43: $e^{-\frac{\tau}{\mu_0}}$,($e^{-\frac{\tau}{\lvert\mu\rvert}}$)	6S
GTF	Gaseous transmission (H2O, O3 and others)	θ_S, θ_V, U_{H2O},U_{O3}	Equation **55**: $T_{Msat}^{gas}(i; U_{H2O}, U_{O3})$	6S
IDTF	Incoming diffuse transmission factor for sun	θ_S τ	Equation 49 it is the first term of $S^{ms}(\mu_0)$	6S
SFLA	Used for multiple scattering parameterization	θ_V k, Θ, τ	Equation 51: a(-μ)	6S
SFUA	Used for multiple scattering parameterization	θ_V k, Θ	Equation 50: A(-μ)	6S
STF	Transmission factors for upward and downward scattered radiation	θ_S, θ_V k, Θ, τ	Equation 45 (all 6 integrals)	6S
DHR30	Angular term of the DHR@ 30°	k, Θ	Equation 16 and Equation 25	RPV
DRHErr	DHR Error	k, Θ		[RD 10]
k: 0.4, 0.5, 0.6, 0.7, 0.8, 0.9, 1.0 **Θ**: –0.30, –0.25, –0.20, –0.15, –0.10, –0.05, 0.00 **τ** : 0.1, 0.2, 0.3, 0.4, 0.6, 0.8, 1.0			θ_S, θ_V,: Sun angle, View angle varying from 0° – 70° with increments of 2° Δφ: difference azimuth angle varies from 0° – 180° with increments of 10°.	

Table 11: List of Look-up Tables in the CRAF database

APPENDIX C NUMERICAL COMPUTATION ASPECTS

All integrals mentioned in the ATBD are solved numerically using a Gaussian quadrature method:

$$I = \int_a^b f(x)\,dx \approx \sum_{i=1}^{n} f\left[x(i)\right] w(i) \qquad \textit{Equation 106}$$

where:

$x(i)$	are the n Gaussian points estimated between a and b
$w(i)$	are the associated weights

The values of these points and weights are computed using the GAULEG procedure described in [RD 26].

C.1 Computations of the Fourier coefficients

The first two Fourier coefficients appearing in the generic Equation 40 and Equation 41 are obtained from an integration of the appropriate angular function over the relative azimuth between 0 and 2π. The GAULEG procedure calls for $a = 0$ and $b = 2\pi$, respectively, using 48 points of a Gauss quadrature. Equation 40 and Equation 41 are then rewritten as follows:

$$Y_0(\mu', -\mu) = \frac{1}{2\pi} \sum_{i=1}^{48} Y\left[\mu', -\mu, \phi_{Gauss}(i)\right] w_{\phi_{Gauss}}(i) \qquad \textit{Equation 107}$$

and:

$$Y_1(\mu', -\mu) = \frac{1}{\pi} \sum_{i=1}^{48} Y\left[\mu', -\mu, \phi_{Gauss}(i)\right] \cos\left[\phi_{Gauss}(i)\right] w_{\phi_{Gauss}}(i) \qquad \textit{Equation 108}$$

C.2 Computations of the STF functions

The STF dataset contains the values of the $f_{0,1}$, $g_{0,1}$ and the $h_{0,1}$ functions. These functions (Equation 45) correspond to integrals over cosine angles taken between 0 and 1. The Gauss method was then applied with $a = 0$ and $b = 1$ using 24 Gaussian quadrature points. The generic formulation used to estimate the values of the f_0, g_0 and h_0 functions is as follows:

$$F_0(\mu_1, \mu_2) = 2\pi \sum_{i=1}^{24} T_0\left[\mu_1, \mu_{Gauss}(i)\right] p_0\left[\mu_{Gauss}(i), \mu_2\right] \mu_{Gauss}(i)\, w_{\mu_{Gauss}}(i) \qquad \textit{Equation 109}$$

where the generic functions and variables are defined as follows:

Generic variable	F_0	μ_1	μ_2	P_0
Specific variable	f_0	μ_0	$-\mu$	r_0
	g_0	$-\mu$	μ_0	r_0
	h_0	μ_0	$-\mu$	f_0

APPENDIX D LIST OF THE SELECTABLE PARAMETERS

The following tables summarize the numerical values of selectable parameters required in the retrievals of surface albedo values. The values indicated in Table 12, Table 13, Table 14 and Table 15 correspond to the default values set in the prototype version of the Meteosat Surface Albedo algorithm. They define a kind of standard and most common set of values for the (M)RPV model.

Parameter Identification	*Value*
Threshold for the maximum Solar zenith angle value	70˚
Maximum acceptable value for data smoothness, σ_{DCP}	10 % of the averaged Meteosat BRF values
Threshold value for χ^2_{DCP}	1.0
Threshold value for the minimum number of required slots	6
Maximum value of R_0 in the MRPV model	1.0
Minimum value of R_0 in the MRPV model	0.0
Maximum value of k_M in the MRPV model	1.2
Minimum value of k_M in the MRPV model	0.0
Maximum value of b_M in the MRPV model	1.2
Minimum value of b_M in the MRPV model	–1.2

Table 12: Numerical values of the selectable parameters in the DCP

Parameter Identification	*Value*
Weighting functions, $W_{inv}(i)$, in the inverse function	1.0
$\hat{\rho}_c$ value to use in the hot spot factor	0.15
Maximum value of $\tilde{\rho}$ in the RPV model	1.0
Minimum value of $\tilde{\rho}$ in the RPV model	0.0

Table 13: Numerical values of the selectable parameters in the ASM

Parameter Identification	*Value*
Maximum value of the average deviations for the retrievals	1.0
Minimum value of the average deviations for the retrievals	0.0
Convergence criterion for retrieving $\tilde{\rho}_0$ by iteration	10^{-3}
Maximum number of iteration allowed to estimate $\tilde{\rho}_0$	10
Maximum value of the “Likely” $\hat{\rho}$ value	1.0
Minimum value of the "Likely" $\hat{\rho}$ value	0.0
Maximum value of the DHR	1.0
Minimum value of the DHR	0.0
Maximum value of the BHR_{iso}	1.0
Minimum value of the BHR_{iso}	0.0

Table 14: Numerical values of the selectable parameters in the DIM

Parameter Identification	*Value*
Number of days used to estimate temporally averaged quantities	10

Table 15: Numerical values of the selectable parameters in the SAM

APPENDIX E MATHEMATICAL SYMBOLS AND SHORTHAND USED IN THIS DOCUMENT

E.1 Generic Notation

Symbol	*Meaning*
$\hat{x}$	"Likely" value of the x parameter
Δ_x	Average deviation of the distribution of acceptable values for the parameter x
$\bar{x}$	Arithmetic mean of the x values
$x^{\Uparrow}$	Radiance travelling upward in the atmosphere
$x^{\Downarrow}$	Radiance travelling downward in the atmosphere
$x^{\uparrow}$	Radiance travelling upward in the scattering-only atmosphere
$x^{\downarrow}$	Radiance travelling downward in the scattering-only atmosphere
$\overline{\hat{x}}$	Temporal average of the "Likely" values of the x parameter
$\{\hat{x}\}$	Most representative value among the set of the ('Likely" values of the *x* parameter)
$[\hat{x}]$	Spatial average of the "Likely" values of the *x* parameter
X	vector
$\hat{x}$	estimation of x
σ_x	error of x
$\langle x \rangle$	average of x.
P(x)	probability of x

Table 16: Generic Notion

E.2 Greek Symbols Used in Notation

Symbol	*Meaning*
α_0	Spherical angular average of the surface BRF angular function
x^2_{DCP}	χ^2 function for BRF data smoothness
λ	Wavelength
μ'	Cosine of the zenith angle of observation
α_0	Cosine of the zenith angle of any arbitrary direction
μ_0	Cosine of the zenith angle of Sun
Ω	Direction of observation
Ω', Ω"	Any arbitrary direction of origin of the radiation
Ω_0	Direction of solar illumination
ρ_0	Parameter describing the amplitude of the surface BRF in the RPV model
ρ_c	Parameter describing the amplitude of the hot spot formulae in the RPV model

Symbol	*Meaning*
$\rho_{sfc}(z_0, \Omega' \rightarrow \Omega)$	Surface BRF for illumination from direction fl'
$\rho_{sfc}(z_0, \Omega_0 \rightarrow \Omega)$	Surface BRF for illumination from the solar direction
$\rho_{sfc}(z_{soa}, \Omega_0 \rightarrow \Omega)$	Surface contribution to the BRF of the scattering-only-atmosphere
$\breve{\rho}_{sfc}(z_0, \Omega' \rightarrow \Omega)$	Angular function of the surface BRF
$\breve{\rho}_{sfc}(z_{soa}, \Omega' \rightarrow \Omega)$	Angular function of the BRF at the top of the scattering-only-atmosphere
$\rho^{ms}(-\mu, \mu^0)$	BRr contribution due to multiple scattering effects between the atmosphere and surface
σ_{act}	Root mean square of the fit of the MRPV model
σ_{DCP}	maximum value allowed for q (let
σ_{data}	Standard deviation in the Meteosat data and model predicted BRF values
τ	Spectral atmospheric optical depth
Θ_{HG}	Parameter describing the asymmetry of the BRF in the RPV model
θ_0	Solar zenith angle
θ_v	Satellite zenith angle
φ	Sun-Satellite relative azimuth
α	aerosol temporal autocorrelation
β	random noise
κt	normalized weight for the estimation of $\overline{\rho}0$ and $\sigma\ \overline{\rho}0$
κT	normalized weight for the estimation of $\sigma\ \hat{x}$
ν	number of degree of freedom of the cost function
$\rho 0$	amplitude of the surface BRF
$\overline{\rho}0$	weighted mean value of ρ0 for all acceptable solutions.
ρa	intrinsic reflectance of the scattering layer
ρs	reflectance at the surface.
$\breve{\rho}s$	angular field of the BRF
$\sigma\overline{\rho}0$	weighted standard error $\overline{\rho}0$.
$\sigma p1$	root mean square error between the landmarks and their actual position on the earth along the E-W direction
$\sigma p2$	root mean square error between the landmarks and their actual position on the earth along the N-S direction
$\sigma_{K1.5}$	instrument radiometric noise for level 1.5 images
$\sigma\ \overline{K}0$	mean space count standard deviation
$\rho 0$	amplitude of the surface BRF
σ_{ξ}	calibration error due to the uncertainty in SSR

Symbol	*Meaning*
σ_ι	calibration error due to the residual random effects
σ_λ	error from the DHR spectral conversion.
σ_{DHR}	random error on the estimation of the DHR
σ_{DRH}^{T}	total (random+systematic) DHR error
τ	equivalent aerosol optical thickness.
χ^2	cost function
χ_{Ny}^2	normalized cost function
χ_a^2	cost function threshold value for the acceptable solutions
Γ	Gamma function
Θ	parameter describing the asymmetry of the BRF in the RPV model
Ω_s	illumination direction
μ_s	cosine of the illumination zenith angle
Φ_s	illumination azimuth angle
Ω_v	viewing direction
μ_v	cosine of the viewing zenith angle
Φ_s	viewing azimuth angle
Ω'	any arbitrary direction

Table 17: Greek symbols used in notation

E.3 Upper-Case Roman Symbols Used in Notation

Symbol	*Meaning*
$A(-\mu)$	Plane angular average of the BRF angular function
BHR^*	Bi-hemispherical reflectance (Blue sky albedo)
BHR_{iso}	Bi-hemispherical reflectance for isotropic illumination (White sky albedo)
DHR	Directional hemispherical reflectance (Black sky albedo)
$E\uparrow(z_0, \mu_0)$	Spectral radiant exitance at the surface level
$E\downarrow(z_0, \mu_0)$	Spectral surface irradiance
G	Geometrical parameter entering the hot spot formulae
$H(\overline{R_{Msat}}, G)$	Hot spot function in the :VIRPV model
$I^{\downarrow}(z_0, \Omega', \Omega_0)$	Spectral downwelling radiance
$I^{\uparrow}(z_0, \Omega, \Omega_0)$	Spectral upwelling radiance
$I_{Msat}^{\Uparrow}(z_{sat}, \Omega, \Omega_0)$	Radiance measured by the Meteosat sensor
$I_{atm}^{\Uparrow}(z_{sat}, \Omega, \Omega_0)$	Spectral radiance intrinsic to the atmosphere
$I_{sfc}^{\Uparrow}(z_{sat}, \Omega, \Omega_0)$	Spectral radiance due to the coupled surface-atmosphere system at the

Symbol	*Meaning*
	satellite level
$I^{\uparrow}_{atm}(z_{soa}, \Omega, \Omega_0)$	Spectral radiance intrinsic to the scattering-only atmosphere
$I^{\uparrow}_{sfc}(z_{soa}, \Omega, \Omega_0)$	Upwelling spectral radiance due to the surface-scattering-only atmosphere
$I^{\downarrow}_{sfc}(z_0, \Omega', \Omega_0)$	Downwelling spectral radiance reaching the surface in the scattering-only atmosphere
$\overline{K}_{0n}$	Mean space count for the detector n
K	Digital count value
$\overline{K}_0$	Mean space count value
L_a	Ensemble of acceptable solutions
L_a	Number of solutions in La
$\mathcal{L}_{\sigma y}$	Ensemble of solutions defined by the uncertainty of the retrieval
N_T	Number of days with an acceptable solution during the composite period
N_y	Size of measurement vector
P_a	Threshold probability for the ensemble of acceptable solutions
$\mathbf{P}_{\sigma y}$	Threshold probability determined by measurement error
R_n	Radiometer on board the Meteosat series number n
$S(\lambda)$	Meteosat spectral response
S	Spherical albedo of the atmosphere
$S^{ms}(\mu_0)$	Source term at the surface level due to the multiple surface-atmosphere interaction
T	Number of days used to estimate the temporally averaged quantities transmission factor of the scattering-only atmosphere
T_0	Total spectral atmospheric transmission factor in direction n of the upwelling radiance field in the direction on
T_1	Spectral transmission factor in direction of the upwelling radiance field scattered by the surface in direction 0.
T_g	gaseous transmittance
$T^{\Uparrow}(\Omega'', \Omega)$	Spectral transmission factor for the downward radiation in the scattering-only-atmosphere
$T^{\uparrow}(\Omega'', \Omega)$	Spectral transmission factor due to the absorbing gases only
$T^{\downarrow}(\Omega'', \Omega)$	Transmission factor due to the absorbing gases only weighted by the Meteosat spectral response
U_{H2O}	Total column water vapour concentration
U_{O3}	Total column ozone concentration

Table 18: Roman Symbols Upper Case

E.3 Lower-Case Roman Symbols Used in Notation

Symbol	*Meaning*
aμ	Plane angular average of the BRi angular function weighted by the incoming atmospherically-scattered radiation
i	Index of the current slot
k	Parameter describing the bowl shape of the BRF in the RPV model
k_M	Parameter describing the bowl shape of the BRF in the MRPV model
b_M	Parameter describing the asymmetry of the BRF shape in the MRPV model
$f_{0,1}$	Coupled surface-atmosphere contribution due to the incoming atmospherically scat-tered radiation transmitted directly to the satellite
$g_{0,1}$	Coupled surface-atmosphere contribution due to the incoming direct radiation scattered by the surface-atmosphere system to the satellite
g	Phase angle between the directions of illumination and observation
$h_{0.1}$	Coupled surface-atmosphere contribution due to the incoming atmospherically scattered radiation scattered by the surface-atmosphere system to the satellite
r_0	First term of the Fourier expansion in relative azimuth angle of angular function of the surface BRF
r_1	Second term of the Fourier expansion in relative azimuth angle of angular function of the surface BRF
z_0	Level of the surface
z_{sat}	Level of the satellite
z_{son}	Level of the Scattering-Only-Atmosphere
b	number of digitalization bits
d	day number within the 10-day compositing period
k	parameter describing the bowl shape of the BRF in the RPV model
n	detector number
p_1	position of a pixel along a line
p_2	position of a pixel along a column
t	time of acquisition of a line of pixels
$t_{Pa/2}$	Student coefficient for the 2-tails distribution
y	forward model
z_0	bottom of the atmosphere
z_s	top of the gaseous absorption layer

Symbol	*Meaning*
z_a	top of the scattering-only layer

Table 19: Roman Symbols Lower-Case used in notation

E.4 Vector Symbols Used in Notation

Symbol	*Meaning*
b	model parameters
x	state vector
$\mathbf{x}_s$	parameters representing surface properties of state vector
$\mathbf{y}_m$	measurement vector
$\hat{\mathbf{x}}$	most representative solution for the 10-day period
σ_y	total measurement error
$\sigma_{\hat{\mathbf{x}}}$	retrieved error for the one day solution ^
$\sigma_{\bar{\hat{\mathbf{x}}}}$	retrieved error for the 10-day period solution
σ_A	aerosol daily correlation error
σ_1	measurement radiometric error
σ_D	digitalization error
σ_R	rectification uncertainty
σ_F	forward model error

Table 20: Vector Symbols